Accepted for publication in The Astrophysical Journal

Search for Gamma-ray Emission from X-ray Selected Seyfert Galaxies with *Fermi*–LAT

M. Ackermann[2], M. Ajello[2], A. Allafort[2], L. Baldini[3], J. Ballet[4], G. Barbiellini[5,6], D. Bastieri[7,8], K. Bechtol[2,1], R. Bellazzini[3], B. Berenji[2], E. D. Bloom[2], E. Bonamente[9,10], A. W. Borgland[2], J. Bregeon[3], M. Brigida[11,12], P. Bruel[13], R. Buehler[2], S. Buson[7,8], G. A. Caliandro[14], R. A. Cameron[2], P. A. Caraveo[15], J. M. Casandjian[4], E. Cavazzuti[16], C. Cecchi[9,10], E. Charles[2], A. Chekhtman[17], C. C. Cheung[18], J. Chiang[2], S. Ciprini[19,10], R. Claus[2], J. Cohen-Tanugi[20], J. Conrad[21,22,23], S. Cutini[16], F. D'Ammando[24,25], A. de Angelis[26], F. de Palma[11,12], C. D. Dermer[27], E. do Couto e Silva[2], P. S. Drell[2], A. Drlica-Wagner[2], T. Enoto[2], C. Favuzzi[11,12], S. J. Fegan[13], E. C. Ferrara[28], P. Fortin[13], Y. Fukazawa[29], P. Fusco[11,12], F. Gargano[12], D. Gasparrini[16], N. Gehrels[28], S. Germani[9,10], N. Giglietto[11,12], P. Giommi[16], F. Giordano[11,12], M. Giroletti[30], G. Godfrey[2], J. E. Grove[27], S. Guiriec[31], D. Hadasch[14], M. Hayashida[2,32,1], E. Hays[28], R. E. Hughes[33], G. Jóhannesson[34], A. S. Johnson[2], T. Kamae[2], H. Katagiri[35], J. Kataoka[36], J. Knödlseder[37,38], M. Kuss[3], J. Lande[2], M. Llena Garde[21,22], F. Longo[5,6], F. Loparco[11,12], B. Lott[39], M. N. Lovellette[27], P. Lubrano[9,10], G. M. Madejski[2,1], M. N. Mazziotta[12], P. F. Michelson[2], T. Mizuno[29], C. Monte[11,12], M. E. Monzani[2], A. Morselli[40], I. V. Moskalenko[2], S. Murgia[2], S. Nishino[29], J. P. Norris[41], E. Nuss[20], M. Ohno[42], T. Ohsugi[43], A. Okumura[2,42], E. Orlando[2,44], M. Ozaki[42], D. Paneque[45,2], M. Pesce-Rollins[3], M. Pierbattista[4], F. Piron[20], G. Pivato[8], T. A. Porter[2,2], S. Rainò[11,12], R. Rando[7,8], M. Razzano[3,46], A. Reimer[47,2], O. Reimer[47,2], S. Ritz[46], M. Roth[48], D.A. Sanchez[49], C. Sbarra[7], C. Sgrò[3], E. J. Siskind[50], G. Spandre[3], P. Spinelli[11,12], Ł. Stawarz[42,51,1], A. W. Strong[44], H. Takahashi[43], T. Takahashi[42], T. Tanaka[2], J. B. Thayer[2], D. J. Thompson[28], L. Tibaldo[7,8], M. Tinivella[3], D. F. Torres[14,52], G. Tosti[9,10], E. Troja[28,53], Y. Uchiyama[2], T. L. Usher[2], J. Vandenbroucke[2], V. Vasileiou[20], G. Vianello[2,54], V. Vitale[40,55], A. P. Waite[2], B. L. Winer[33], K. S. Wood[27], M. Wood[2], Z. Yang[21,22], S. Zimmer[21,22]

[1]Corresponding authors: M. Hayashida, mahaya@slac.stanford.edu; Ł. Stawarz, stawarz@astro.isas.jaxa.jp; K. Bechtol, bechtol@stanford.edu; G. M. Madejski, madejski@slac.stanford.edu.

[2]W. W. Hansen Experimental Physics Laboratory, Kavli Institute for Particle Astrophysics and Cosmology, Department of Physics and SLAC National Accelerator Laboratory, Stanford University, Stanford, CA 94305, USA

[3]Istituto Nazionale di Fisica Nucleare, Sezione di Pisa, I-56127 Pisa, Italy

[4]Laboratoire AIM, CEA-IRFU/CNRS/Université Paris Diderot, Service d'Astrophysique, CEA Saclay, 91191 Gif sur Yvette, France

[5]Istituto Nazionale di Fisica Nucleare, Sezione di Trieste, I-34127 Trieste, Italy

[6]Dipartimento di Fisica, Università di Trieste, I-34127 Trieste, Italy

[7]Istituto Nazionale di Fisica Nucleare, Sezione di Padova, I-35131 Padova, Italy

[8]Dipartimento di Fisica "G. Galilei", Università di Padova, I-35131 Padova, Italy

[9]Istituto Nazionale di Fisica Nucleare, Sezione di Perugia, I-06123 Perugia, Italy

[10]Dipartimento di Fisica, Università degli Studi di Perugia, I-06123 Perugia, Italy

[11]Dipartimento di Fisica "M. Merlin" dell'Università e del Politecnico di Bari, I-70126 Bari, Italy

[12]Istituto Nazionale di Fisica Nucleare, Sezione di Bari, 70126 Bari, Italy

[13]Laboratoire Leprince-Ringuet, École polytechnique, CNRS/IN2P3, Palaiseau, France

[14]Institut de Ciències de l'Espai (IEEE-CSIC), Campus UAB, 08193 Barcelona, Spain

[15]INAF-Istituto di Astrofisica Spaziale e Fisica Cosmica, I-20133 Milano, Italy

[16]Agenzia Spaziale Italiana (ASI) Science Data Center, I-00044 Frascati (Roma), Italy

[17]Artep Inc., 2922 Excelsior Springs Court, Ellicott City, MD 21042, resident at Naval Research Laboratory, Washington, DC 20375

[18]National Research Council Research Associate, National Academy of Sciences, Washington, DC 20001, resident at Naval Research Laboratory, Washington, DC 20375

[19]ASI Science Data Center, I-00044 Frascati (Roma), Italy

[20]Laboratoire Univers et Particules de Montpellier, Université Montpellier 2, CNRS/IN2P3, Montpellier, France

[21]Department of Physics, Stockholm University, AlbaNova, SE-106 91 Stockholm, Sweden

[22]The Oskar Klein Centre for Cosmoparticle Physics, AlbaNova, SE-106 91 Stockholm, Sweden

[23]Royal Swedish Academy of Sciences Research Fellow, funded by a grant from the K. A. Wallenberg Foundation

[24]IASF Palermo, 90146 Palermo, Italy

[25]INAF-Istituto di Astrofisica Spaziale e Fisica Cosmica, I-00133 Roma, Italy

[26]Dipartimento di Fisica, Università di Udine and Istituto Nazionale di Fisica Nucleare, Sezione di Trieste, Gruppo Collegato di Udine, I-33100 Udine, Italy

[27]Space Science Division, Naval Research Laboratory, Washington, DC 20375-5352

[28]NASA Goddard Space Flight Center, Greenbelt, MD 20771, USA

[29]Department of Physical Sciences, Hiroshima University, Higashi-Hiroshima, Hiroshima 739-8526, Japan

[30]INAF Istituto di Radioastronomia, 40129 Bologna, Italy

[31]Center for Space Plasma and Aeronomic Research (CSPAR), University of Alabama in Huntsville, Huntsville, AL 35899

[32]Department of Astronomy, Graduate School of Science, Kyoto University, Sakyo-ku, Kyoto 606-8502, Japan

[33]Department of Physics, Center for Cosmology and Astro-Particle Physics, The Ohio State University, Columbus, OH 43210, USA

[34]Science Institute, University of Iceland, IS-107 Reykjavik, Iceland

[35]College of Science, Ibaraki University, 2-1-1, Bunkyo, Mito 310-8512, Japan

[36]Research Institute for Science and Engineering, Waseda University, 3-4-1, Okubo, Shinjuku, Tokyo 169-8555, Japan

[37]CNRS, IRAP, F-31028 Toulouse cedex 4, France

[38]GAHEC, Université de Toulouse, UPS-OMP, IRAP, Toulouse, France

[39]Université Bordeaux 1, CNRS/IN2p3, Centre d'Études Nucléaires de Bordeaux Gradignan, 33175 Gradignan, France

[40]Istituto Nazionale di Fisica Nucleare, Sezione di Roma "Tor Vergata", I-00133 Roma, Italy

[41]Department of Physics, Boise State University, Boise, ID 83725, USA

[42]Institute of Space and Astronautical Science, JAXA, 3-1-1 Yoshinodai, Chuo-ku, Sagamihara, Kanagawa 252-5210, Japan

[43]Hiroshima Astrophysical Science Center, Hiroshima University, Higashi-Hiroshima, Hiroshima 739-8526, Japan

[44]Max-Planck Institut für extraterrestrische Physik, 85748 Garching, Germany

[45]Max-Planck-Institut für Physik, D-80805 München, Germany

[46]Santa Cruz Institute for Particle Physics, Department of Physics and Department of Astronomy and Astrophysics, University of California at Santa Cruz, Santa Cruz, CA 95064, USA

[47]Institut für Astro- und Teilchenphysik and Institut für Theoretische Physik, Leopold-Franzens-Universität Innsbruck, A-6020 Innsbruck, Austria

[48]Department of Physics, University of Washington, Seattle, WA 98195-1560, USA

ABSTRACT

We report on a systematic investigation of the γ-ray properties of 120 hard X-ray–selected Seyfert galaxies classified as 'radio-quiet' objects, utilizing the three-year accumulation of *Fermi*–LAT data. Our sample of Seyfert galaxies is selected using the *Swift*–BAT 58-month catalog, restricting the analysis to the bright sources with average hard X-ray fluxes $F_{14-195\,\mathrm{keV}} \geq 2.5 \times 10^{-11}\,\mathrm{erg\,cm^{-2}\,s^{-1}}$ at high Galactic latitudes ($|b| > 10°$). In order to remove 'radio-loud' objects from the sample, we use the 'hard X-ray radio loudness parameter', R_{rX} , defined as the ratio of the total 1.4 GHz radio to $14 - 195$ keV hard X-ray energy fluxes. Among 120 X-ray bright Seyfert galaxies with $R_{\mathrm{rX}} < 10^{-4}$, we did not find a statistically significant γ-ray excess ($TS > 25$) positionally coincident with any target Seyferts, with possible exceptions of ESO 323–G077 and NGC 6814. The mean value of the 95 % confidence level γ-ray upper limit for the integrated photon flux above 100 MeV from the analyzed Seyferts is $\simeq 4 \times 10^{-9}\,\mathrm{ph\,cm^{-2}\,s^{-1}}$, and the upper limits derived for several objects reach $\simeq 1 \times 10^{-9}\,\mathrm{ph\,cm^{-2}\,s^{-1}}$. Our results indicate that no prominent γ-ray emission component related to active galactic nucleus activity is present in the spectra of Seyferts around GeV energies. The *Fermi*–LAT upper limits derived for our sample probe the ratio of γ-ray to X-ray luminosities $L_\gamma/L_{\mathrm{X}} < 0.1$, and even < 0.01 in some cases. The obtained results impose novel constraints on the models for high energy radiation of 'radio-quiet' Seyfert galaxies.

Subject headings: accretion, accretion disks — galaxies: active — galaxies: Seyfert — gamma rays: galaxies — X-rays: galaxies

[49]Max-Planck-Institut für Kernphysik, D-69029 Heidelberg, Germany

[50]NYCB Real-Time Computing Inc., Lattingtown, NY 11560-1025, USA

[51]Astronomical Observatory, Jagiellonian University, 30-244 Kraków, Poland

[52]Institució Catalana de Recerca i Estudis Avançats (ICREA), Barcelona, Spain

[53]NASA Postdoctoral Program Fellow, USA

[54]Consorzio Interuniversitario per la Fisica Spaziale (CIFS), I-10133 Torino, Italy

[55]Dipartimento di Fisica, Università di Roma "Tor Vergata", I-00133 Roma, Italy

1. Introduction

The all-sky observations of celestial objects by the Large Area Telescope (LAT: Atwood et al. 2009) aboard the *Fermi* Gamma-ray Space Telescope confirmed that, in addition to Gamma-ray Bursts, there are at least two more general classes of bright extragalactic sources of γ-rays (Abdo et al. 2010b). One class comprises Active Galactic Nuclei (AGN) with powerful relativistic jets, including blazars, radio-loud Narrow-line Seyfert 1 galaxies (NLS1s), and radio galaxies, which produce beamed high-energy emission via inverse-Compton scattering of soft photon fields on ultra-relativistic jet electrons. The other class consists of nearby galaxies with prominent starburst systems, which produce diffuse, un-beamed γ-ray emission resulting from the interactions of cosmic-ray particles with the interstellar medium (ISM). An important question arises whether those are the only classes of extragalactic γ-ray sources. This question motivated us to search systematically for GeV emission from Seyfert galaxies using *Fermi*–LAT. Seyfert galaxies constitute the most numerous class of AGN in the local Universe (local number density $\sim 10^{-4}\,\mathrm{Mpc}^{-3}$), but at the same time lack, in general, ultrarelativistic collimated outflows or starburst regions (e.g., Osterbrock 1989). Seyferts, hosted by late-type galaxies, were originally identified in the optical regime by the presence of strong emission lines from highly ionized gas in their spectra (Seyfert 1943). They are believed to harbor super-massive ($\mathcal{M}_{\mathrm{BH}} \sim 10^6 - 10^9\,M_{\odot}$; see e.g., Ho 2002) black holes in their galactic centers, and are powered by the infalling matter which forms accretion disks emitting intense optical/UV continuum radiation.

Seyfert galaxies are generally much weaker radio emitters than radio quasars or radio galaxies, but they are not 'radio silent'. In addition to the diffuse radio continuum originating in the ISM of their late-type hosts, about half of the nearby Seyferts possess compact non-thermal radio cores (Ulvestad & Wilson 1989; Kukula et al. 1995; Ho & Ulvestad 2001), which are often accompanied by arcsecond-scale jets and jet-like features (e.g., Middelberg et al. 2004; Gallimore et al. 2006; Lal et al. 2011). However, the radio cores and jets witnessed in Seyferts are generally very different from those observed in radio quasars or radio galaxies. In particular, radio cores in Seyfert galaxies are characterized by only modest brightness temperatures (see, e.g., Ulvestad & Ho 2001; Ho 2008), and in general, show no indication of relativistic beaming.

Some Seyfert galaxies also display broad permitted emission lines in their spectra. Presence of such lines anti-correlates with the obscuration of unresolved cores in the optical–to–soft X-ray regime. This fact led to the idea that objects either possessing or lacking broad lines are intrinsically the same, differing only in the orientation of the central engine to the line of sight due to the selective absorption of the core emission by the anisotropically distributed circumnuclear dust (the so-called 'unification scheme'; Antonucci 1993). Hence

broad-line Seyferts are called 'unobscured' (or 'type 1'), while Seyferts without broad emission lines in their spectra are called 'obscured' (or 'type 2'). One should note that there are several intermediate classes of Seyferts with respect to the nuclear obscuration (type 1.2, 1.5, etc. Osterbrock 1977), as well as the objects which intrinsically lack broad emission lines (NLS1s; e.g., Pogge 2000; Foschini et al. 2011a).

While optical information is needed for proper classification of an astrophysical source as an AGN, X-ray characteristics are equally important in understanding the physics of central engines in active galaxies. Seyfert galaxies are ubiquitous X-ray emitters (e.g., Ho et al. 2001; Terashima & Wilson 2003; Cappi et al. 2006), and the class is generally known to be particularly bright in the hard X-ray regime (above 10 keV; see, e.g., Tueller et al. 2008; Beckmann et al. 2009). This hard X-ray emission, typically in a form of a power-law continuum (photon indices $\Gamma_X \simeq 2$) cutting-off around a few hundred keV (Gondek et al. 1996; Zdziarski et al. 2000), is well understood as being due to optical/UV disk emission reprocessed in the clumpy, hot, but predominantly thermal coronae of accretion disks (see, e.g., Poutanen 1998; Zdziarski 1999, for reviews).

On the other hand, spectral properties of Seyfert galaxies in the γ-ray regime (and especially at high- and very-high-energy γ-rays, i.e. at GeV–TeV photon energy ranges) are basically unknown because of the limited sensitivity of past γ-ray instruments. The upper limits derived using observations by the the Imaging Compton Telescope (COMPTEL: Schoenfelder et al. 1993) onboard the Compton Gamma-Ray Observatory (CGRO) are consistent with no significant emission component around 1 MeV (Maisack et al. 1995, 1997). Similarly, observations with the Energetic Gamma-Ray Experiment Telescope (EGRET: Thompson et al. 1993) did not result in any detection of Seyfert galaxies (individually, or as a class by means of a stacking analysis) above 100 MeV (Lin et al. 1993; Cillis et al. 2004). One might therefore conclude that, despite some expectations (see Section 5.2 below) and unlike jet dominated sources (blazars, radio-loud NLS1s, or nearby radio galaxies), Seyferts are particularly 'γ-ray quiet'. This issue can now be addressed more robustly using the *Fermi*–LAT instrument, simply because of its unprecedented sensitivity to photons on the GeV range.

Fermi–LAT has already discovered or confirmed a number of different classes and types of non-blazar γ-ray–emitting AGN, such as NLS1s (Abdo et al. 2009b), low-power FR I radio galaxies (Abdo et al. 2010c), high-power broad-line radio galaxies (Kataoka et al. 2011), and sources hosting 'reborn' compact radio structures (McConville et al. 2011). All these targets appear however to posses relativistic jets aligned relatively closely to the line of sight. Nearby starburst systems have been detected by *Fermi*–LAT as well (Abdo et al. 2010b; Lenain et al. 2010; Ackermann et al. 2011b). However, radio-quiet Seyfert galaxies

lacking a circumnuclear starburst have never been significantly detected as γ-ray sources. We note that, in parallel to our studies, Teng et al. (2011) have reported their analysis of 491 Seyfert galaxies included in the *Swift*–BAT catalog using 2.1 years accumulation of *Fermi*–LAT data in the 1–100 GeV energy range. Teng et al. (2011) found only two objects in their sample, NGC 1068 and NGC 4945, to be significantly detected in the 1–100 GeV energy range. Those two sources have been already reported as γ-ray emitters in the First *Fermi*–LAT Catalog (Abdo et al. 2010b) and discussed in more detail by Lenain et al. (2010), but their GeV emission most likely originates in the ISM of the host galaxies (Ackermann et al. 2011b). In this paper we report on a systematic and detailed investigation of the γ-ray properties of hard X-ray–selected Seyfert galaxies classified as radio-quiet objects, utilizing the three-year accumulation of the *Fermi*–LAT data from 0.1–100 GeV, and report flux limits for individual sources. We also discuss the derived upper limits compared with fluxes in other wavebands for each source. The paper is organized as follows: in § 2 we discuss the sample selection; the *Fermi*–LAT data analysis and the results are presented in § 3 and § 4, respectively; the final discussion of our results are given in § 5.

2. Sample Selection

Observations in hard X-rays are useful for selecting a complete and unbiased sample of Seyfert galaxies because hard X-ray emission is a clear and common signature of AGN activity, as described in the previous section. By contrast, the optical–to–soft X-ray emission of Seyfert galaxies may be subject to severe obscuration by circumnuclear dust, depending upon the orientation of the source to the line of sight. The Burst Alert Telescope (BAT: Barthelmy et al. 2005) onboard the *Swift* satellite has provided all-sky survey data in the hard X-ray band with unprecedented high sensitivity, which are well-suited for our investigation given the similar observational strategies of *Swift*–BAT and *Fermi*–LAT . During the last five years of the *Swift*–BAT observations, about seven hundred AGN and galaxies were detected above 15 keV (Baumgartner et al. 2010; Cusumano et al. 2010). Notably, Seyferts outnumber the other classes of AGN detected in the hard X-ray band.

For this project we have selected a sample of the hard X-ray brightest Seyfert galaxies using the most recent version of the publicly available *Swift*–BAT 58-month catalog[1], restricting the analysis to sources with average $14 - 195\,\mathrm{keV}$ fluxes equal to or greater than $2.5 \times 10^{-11}\,\mathrm{erg\,cm^{-2}\,s^{-1}}$. Such hard X-ray flux selection returns 179 non-blazar type AGN which are classified as either 'galaxies' or 'Seyfert galaxies' in the *Swift*–BAT 58-month

[1]http://heasarc.gsfc.nasa.gov/docs/swift/results/bs58mon/

catalog. From these, we excluded sources located close to the Galactic Plane, specifically those within Galactic latitudes $|b| < 10^\circ$ for the Galactic longitudes $|l| > 20^\circ$, and $|b| < 20^\circ$ for $-20^\circ < l < 20^\circ$, because *Fermi*–LAT sensitivity is reduced towards the Galactic plane due to substantial foreground emission related to the ISM of our Galaxy, and presence of numerous Galactic γ-ray emitters (Abdo et al. 2010b). All selected sources are also included in another independent *Swift*–BAT catalog: the Palermo *Swift*–BAT 54-month catalog (Cusumano et al. 2010).

The constructed sample is contaminated by several objects with bright relativistic jets such as nearby radio galaxies (e.g., Centaurus A) and radio-loud quasars, which can be classified also as Seyferts based on their emission line spectral properties in the optical band. All such sources should be removed from the analyzed sample, since those AGN are physically distinct from 'classical' Seyferts. In principle, this could be accomplished by investigating the 'radio loudness' parameter for the selected targets, i.e. the ratio between the monochromatic 5 GHz radio and B-band optical fluxes, $R_{\rm rB} \equiv F_{5\,{\rm GHz}}/F_{\rm B}$. This parameter is often used to distinguish radio-loud ($R_{\rm rB} > 10$) from radio-quiet ($R_{\rm rB} < 10$) quasars, according to the criteria proposed by Kellermann et al. (1989), and is widely accepted as a useful proxy for the jet production efficiency. However, such an interpretation holds *only* if the radio fluxes correspond strictly to the jet emission, and the B-band optical fluxes are mainly due to the accretion disk emission. Both the total optical and radio fluxes in Seyferts can be dominated by host galaxies. If no careful subtraction of the starlight emission is performed, all Seyfert galaxies appear to be radio quiet (with $R_{\rm rB} < 10$). Yet when the starlight emission is carefully subtracted, many 'classical' Seyfert galaxies (especially those accreting at lower rates) formally become radio loud, even if core radio fluxes are used instead of the total radio fluxes, as demonstrated first by Ho & Peng (2001), Ho (2002), and discussed further by Sikora et al. (2007). Another problem is that if one is dealing with a mixture of type 1 and type 2 Seyferts, the intrinsic nuclear optical fluxes may be extremely difficult to determine for the obscured (type 2) objects.

For these reasons, we conclude that the standard definition of the radio loudness parameter is not well-suited for our purposes. Instead, we use the 'hard X-ray radio loudness parameter', $R_{\rm rX}$, defined as the dimensionless ratio of monochromatic radio (1.4 GHz) energy flux density to integrated hard X-ray ($14-195$ keV) energy flux density,

$$R_{\rm rX} = \frac{[\nu F_\nu]_{1.4\,{\rm GHz}}}{F_{14-195\,{\rm keV}}}\,. \tag{1}$$

An analogous X-ray radio loudness parameter was first introduced for Seyfert galaxies and Low-Ionization Nuclear Emission-line Regions (LINERs) by Terashima & Wilson (2003), and discussed further by Panessa et al. (2007). However, those authors used X-ray data from a

lower (medium) photon energy range $2-10$ keV, rather than the hard X-ray fluxes considered in this work. Our choice of using the hard X-ray fluxes from the *Swift*–BAT catalog has an advantage of minimizing the effect of a possible absorption of the X-ray emission in obscured (type 2) objects. At the same time, the typical X-ray photon indices of unobscured Seyfert galaxies $\Gamma_X \lesssim 2$ within the medium range (e.g., Zhou & Zhang 2010, claiming $\Gamma_X \approx 1.74 \pm 0.02$ for the $2-10$ keV band) and $\Gamma_X \gtrsim 2$ at hard X-rays (e.g., Ajello et al. 2008, reporting $\Gamma_X \approx 2.23 \pm 0.11$ in the $14-195$ keV band), imply roughly comparable *intrinsic* energy flux densities in both X-ray regimes. Therefore, the radio loudness parameters evaluated using the definition introduced here and the definition of Terashima & Wilson (2003) or Panessa et al. (2007), should be roughly equivalent. On the other hand, in the case of very Compton-thick objects with an intrinsic absorption column density N_H of more than $10^{24.5}\,\mathrm{cm}^{-2}$, even hard X-ray fluxes in the $14-195$ keV are affected by absorption (see e.g., Gilli et al. 2007); hence the radio loudness parameters provided for such sources have to be taken with caution.

In order to evaluate the radio loudness parameter R_{rX} for all the analyzed objects, we gather their total radio fluxes from the literature including catalogs such as NRAO VLA Sky Survey (NVSS; Condon et al. 1998), the VLA Faint Images of the Radio Sky at Twenty-cm (FIRST; Becker et al. 2003), or Parkes Catalogue 1990 (PKSCAT90; Wright & Otrupcek 1990, see Table 1). We use the 1.4 GHz fluxes, because the data in this band have much better coverage than at 5 GHz. In the case of sources for which 1.4 GHz fluxes are not available, we use measurements at other frequencies ($\nu = 0.843$ or 4.86 GHz) (Mauch et al. 2008; Miller et al. 1993), and convert those fluxes F_ν to fluxes at 1.4 GHz as $[\nu F_\nu]_{1.4\,\mathrm{GHz}} = (\nu_{1.4\,\mathrm{GHz}}/\nu)^{1-\alpha}\,[\nu F_\nu]$ assuming a universal radio spectral index $\alpha = 0.7$ for non-blazar type AGN. We note that among the analyzed objects there are seven Seyfert galaxies for which radio data are not available in the literature; the radio loudness parameters for these cannot be thus evaluated.

Figure 1 shows a histogram of the R_{rX} distribution for the Seyfert galaxies selected from the *Swift*–BAT 58-month catalog after the flux and position cuts described above (yellow bars in the figure). For comparison, we also plot the distribution of the R_{rX} parameter derived for classical 'radio-loud' AGN, which are dominated by the beamed emission of relativistic jets. These latter sources are similarly selected from the *Swift*–BAT 58-month catalog, based on the provided BAT classification (blazar or radio-quasar)[2] and hard X-ray fluxes $\geq 2.5 \times 10^{-11}\,\mathrm{erg\,cm^{-2}\,s^{-1}}$. The selected blazars and radio-quasars (blue bars in Figure 1) are characterized by higher values of the radio loudness parameter and different R_{rX} distribution when compared to the analyzed population of Seyferts. As indicated by Figure 1, the critical

[2]they are categorized as 'beamed AGN' in the BAT catalog

value $R_{\rm rX} = 10^{-4}$ may be used to differentiate between the truly radio-loud and radio-quiet objects, and this cut is applied in our analysis further below.

Terashima & Wilson (2003) and Panessa et al. (2007) found that $R_{\rm rB} \sim 10^5 \, R_{\rm rX}$ for Seyferts and low-luminosity AGN using their medium X-ray fluxes. Since the intrinsic energy flux densities in the medium and hard X-ray regimes are expected to be comparable for Seyferts (see discussion above), the hard X-ray loudness parameter value $R_{\rm rX} = 10^{-4}$ roughly corresponds to the 'classical' radio loudness parameter $R_{\rm rB} = 10$. This simple conversion may not be correct in all cases, though. In particular, in the comparison sample of blazars, there are four objects characterized by the 'standard' radio-loudness parameters $R_{\rm rB} > 10$ but $R_{\rm rX} < 10^{-4}$, namely 2MASS J16561677–3302127, QSO B0033+595, Mrk 421, and QSO B0229+200. Three of them are well known 'high-frequency peaked' BL Lac objects (HBLs) for which the X-ray fluxes are uniquely dominated by the synchrotron emission of highly relativistic jets, and as a result their X-ray–defined radio loudness parameters are low. Those are however exceptional objects in the *Swift*–BAT catalog. On the other hand, for some particularly low-luminosity spiral-hosted AGN (such as LINERs), the evaluated X-ray loudness parameters are $R_{\rm rX} > 10^{-4}$, even though such sources lack relativistic jets. This is simply due to the fact that the total radio emission of such AGN is heavily dominated by the ISM, and is therefore relatively pronounced, while the total accretion-related X-ray emission is particularly low due to very low accretion rates in their nuclei. As a result, the evaluated X-ray loudness parameters for low-luminosity AGN accreting at low rates are high (see in this context Terashima & Wilson 2003; Ho & Peng 2001).

In order to check our final sample against contamination by objects containing prominent relativistic jets, first we check 12 sources with relatively high $R_{\rm rX}$ values: $10^{-4.5} < R_{\rm rX} < 10^{-4.0}$. Among them, 8 sources are obscured Seyferts (type 1.8–2), for which relatively high values of $R_{\rm rX}$ could result from the absorption of the X-ray continuum rather than prominent jet activity. The other 4 sources are type 1–1.5, namely Mrk 6, Mrk 1501, NGC 7469 and NGC 4051, for which no prominent relativistic jet is confirmed except for Mrk 1501. Only 4 sources (Mrk 1501, Mrk 348, NGC 3516 and NGC 7213) among our final sample of 120 sources have counterparts in the CRATES catalog (Healey et al. 2007), which provides a flux-limited all-sky survey of radio core emission. This suggests that most sources in our sample do not have a bright radio core and even the three CRATES Seyferts aside from Mrk 1501 do not display signatures of compact relativistic jets. Therefore, only Mrk 1501 in our sample shows peculiar features and, in fact, the source is known as a 'radio-intermediate' source (e.g., Miller et al. 1993). This galaxy is still worth including in our final sample to address a possible connection between 'classical' radio-loud and radio-quiet AGN. We have thereby confirmed that our sample consists of 'radio-quiet' Seyfert galaxies with a single peculiar 'radio-intermediate' Seyfert object, Mrk 1501.

Finally, we note that two starburst galaxies, NGC 1068 and NGC 4945, which are at the same time high accretion-rate Seyferts (e.g., Lodato & Bertin 2003), and which have been recently detected by *Fermi*–LAT (Abdo et al. 2010b; Lenain et al. 2010; Ackermann et al. 2011b), do not survive the applied cut in the radio loudness parameter, and therefore are not included in the analyzed sample. Both sources are however established Compton-thick objects, with nuclear hydrogen column densities $N_{\rm H} > 10^{24.5}\,{\rm cm}^{-2}$ (e.g., Burlon et al. 2011, and references therein). As noted above, the hard X-ray fluxes of such objects are expected to be affected by nuclear obscuration, and as a result their X-ray radio loudness parameters may — when uncorrected for the absorption — formally read as $R_{\rm rX} > 10^{-4}$. Yet the GeV emission detected from those two sources most likely originates in the ISM of the galactic hosts, as discussed in detail in Ackermann et al. (2011b), even though Lenain et al. (2010) claimed a dominant jet contribution for NGC 1068.

Summarizing, 120 sources are selected for the analysis accordingly to the following criteria:

- hard X-ray fluxes $F_{14-195\,{\rm keV}} \geq 2.5 \times 10^{-11}\,{\rm erg\,cm^{-2}\,s^{-1}}$ in the *Swift*–BAT 58-month catalog;
- spectral classification as 'galaxies' or 'Seyfert galaxies' in the *Swift*–BAT 58-month catalog;
- hard X-ray radio loudness parameters $R_{\rm rX} < 10^{-4}$;
- Galactic coordinates $|b| > 10^\circ$ for $|l| > 20^\circ$, and $|b| > 20^\circ$ for $-20^\circ < l < 20^\circ$.

Table 1 provides source information for the constructed sample of objects including 62 Seyferts of type 1–1.5, 55 Seyferts of type 1.8–2, and three low-luminosity Seyferts classified as 'galaxies' in the *Swift*–BAT catalog. The selected sample includes several radio-quiet NLS1s, such as NGC 4051, NGC 5506, and NGC 7314. We emphasize once more that the applied cut in the hard X-ray–defined radio loudness parameter results in the rejection of not only truly radio-loud AGN, but also some Compton-thick Seyferts or low-luminosity low-accretion rate AGN.

3. *Fermi*–LAT Data Analysis

Fermi–LAT is a pair-production telescope with large effective area ($6500\,{\rm cm}^2$ on axis for > 1 GeV photons) and large field of view (2.4 sr at 1 GeV), sensitive to γ rays in the energy range from 20 MeV to > 300 GeV. Full details of the instrument, as well as of the on-board

and ground data processing, are provided in Atwood et al. (2009). Information regarding on-orbit calibration procedures is given in Abdo et al. (2009a). *Fermi*–LAT normally operates in a scanning 'sky-survey' mode, which provides a full-sky coverage every two orbits (3 hours). For operational reasons, the standard rocking angle (defined as the angle between the zenith and the center of the LAT field of view) for survey mode was increased from 35° to 50° on 2009 September 3.

The data used in this work comprise three years of *Fermi*–LAT observations carried out between August 4, 2008 and August 5, 2011, corresponding to the interval from 239557414 to 334195202 in Mission Elapsed Time (MET). We performed the analysis following the LAT standard analysis procedure[3] using the LAT analysis software, *ScienceTools v9r25v1*, together with the *P7SOURCE_V6* instrument response functions. We discard events with zenith angles $> 100°$ and exclude time periods when the spacecraft rocking angle relative to zenith exceeded 52° to avoid contamination of γ rays produced in the Earth's atmosphere. Events are extracted within a $15° \times 15°$ region of interest (RoI) centered on the position of each object in our sample (listed in Table 2). For our analysis, we accept the events with estimated energies in the range between 100 MeV and 100 GeV.

Gamma-ray fluxes and spectra are determined by performing a binned maximum likelihood fit of model parameters with *gtlike* for events binned in direction and energy. The target objects themselves are modeled as point sources with simple power-law photon spectra $d\mathcal{F}/dE = N \times (E/E_0)^{-\Gamma}$. The background model applied here includes standard models for the isotropic and Galactic diffuse emission components[4]. In addition, the model includes point sources representing all γ-ray emitters within each RoI based on the Second *Fermi*–LAT Catalog (2FGL: Abdo et al. 2011). We examine the significances of γ-ray signals for the analyzed sources by means of their test statistic (TS) values based on the likelihood ratio test (Mattox et al. 1996). If no significant γ-ray excess above background is detected, we derive a 95 % confidence level (CL) upper limit for the integrated photon flux above 100 MeV $\mathcal{F}(> 100\,\mathrm{MeV}) = \int_{100\,\mathrm{MeV}} dE\,(d\mathcal{F}/dE)$, using the Bayesian method (Helene 1983) with a fixed photon index Γ. Here, we assume two values for the photon index: $\Gamma = 2.5$, corresponding to the average photon index for the flux-limited sample of 'flat-spectrum radio quasars' included in the 1st *Fermi*–LAT AGN catalog (1LAC; Abdo et al. 2010a), and $\Gamma = 2.2$, corresponding to the typical γ-ray photon index of LAT-detected starburst galaxies (Ackermann et al. 2011b). These values should be considered as examples only because spectral properties of Seyfert galaxies around GeV photon energies are unknown.

---

[3]see details in http://fermi.gsfc.nasa.gov/ssc/data/analysis/

[4] *'iso_p7v6source.txt'* and *'gal_2yearp7v6_v0.fits'*

4. Results

Our analysis results are summarized in Table 2. We require that two conditions be met in order to claim the detection of γ-ray emission from a target AGN. First, a significant γ-ray excess above backgrounds with $TS > 25$ must be present at the location of the Seyfert as given in the table.[5] Second, we require a positional coincidence defined here as a target AGN existing within the 95 % confidence localization region of the γ-ray excess. Following these criteria, we did not find any significant γ-ray detections among the 120 Seyfert galaxies in our sample, with possible exceptions of ESO 323–G077 and NGC 6814.

TS values above 25 were obtained at the optically-determined locations of ESO 323–G077 and NGC 6814. The γ-ray source 2FGL J1306.9–4028 has been associated with ESO 323–G077 with a probability of 0.8, and 2FGL J1942.5–1024 has been associated with NGC 6814 with 0.91 probability according to the 2FGL catalog and the Second LAT AGN Catalog (2LAC) (Abdo et al. 2011; Ackermann et al. 2011a). The 2FGL catalog warns, however, that "*we expect up to* ~ 2 *false positives among the Seyfert galaxy associations*[6] *(cf. Table 8).*" We consider two possibilities in this work. First, we analyze the RoI under the assumption that ESO 323–G077/NGC 6814 is detected by the LAT as 2FGL J1306.9–4028/2FGL J1942.5–1024. Second, we consider the case in which the proposed associations are actually the result of chance spatial coincidences. In the second case, we compute a flux upper limit at the position of ESO 323–G077/NGC 6814 with 2FGL J1306.9–4028/2FGL J1942.5–1024 included as a background source in the model for the RoI. The proposed associations may be reinforced by more a precise localization given additional exposure, or confirmed by the identification of correlated variability with another waveband. We confirm no significant variability both for 2FGL J1306.9–4028 and 2FGL J1942.5–1024 during the observation period, and find that the spectral shapes are consistent with a simple power law. No blazar in the Roma-BZCAT catalog (Massaro et al. 2009) nor any flat-spectrum radio source in the CRATES catalog (Healey et al. 2007) can be found within $0^\circ.4$ of 2FGL J1306.9–4028 and 2FGL J1942.5–1024.

Figure 2 shows the distribution of resulting upper limits for integrated photon fluxes above 100 MeV, $\mathcal{F}(>100\,\mathrm{MeV})$. For instance, when we assume a photon index of 2.5, the mean value of the γ-ray upper limit from the analyzed Seyferts is $\simeq 4\times10^{-9}\,\mathrm{ph\,cm^{-2}\,s^{-1}}$, and the upper limits derived for several objects are as low as $\simeq 1\times10^{-9}\,\mathrm{ph\,cm^{-2}\,s^{-1}}$. The mean upper limit found with *Fermi*–LAT data is therefore more than two orders of magnitude lower

[5] $TS = 25$ with 2 degrees of freedom corresponds to an estimated $\sim 4.6\,\sigma$ pre-trials statistical significance assuming that the null-hypothesis TS distribution follows a χ^2 distribution (see Mattox et al. 1996).

[6] The 2FGL catalog uses 27651 Seyfert galaxies in its automatic source association pipeline.

than the upper limits derived for the brightest Seyferts based on the *SAS 2* and *COS B* data (Bignami et al. 1979; Pollock et al. 1981, respectively), more than an order of magnitude lower than the analogous EGRET upper limits, $(0.5 - 1.5) \times 10^{-7}\,\mathrm{ph\,cm^{-2}\,s^{-1}}$ (Lin et al. 1993), and close to the lower bound of the effective upper limits from the EGRET stacking data analysis for the brightest 32 Seyfert objects, $(0.3 - 1.5) \times 10^{-8}\,\mathrm{ph\,cm^{-2}\,s^{-1}}$ (Cillis et al. 2004). We note here that Teng et al. (2011) estimated a typical flux upper limit of $\sim 1\times10^{-10}$ $\mathrm{ph\,cm^{-2}\,s^{-1}}$ above 1 GeV for a single source. This is consistent with our results covering the bandpass 0.1–100 GeV when re-scaling our γ-ray upper limits to their bandpass, assuming a power law spectral model with photon index 2.5.

5. Discussion

5.1. Multiwavelength Comparison

The left panel of Figure 3 compares hard X-ray ($14 - 195\,\mathrm{keV}$) energy fluxes to upper limits for the γ-ray ($0.1 - 10\,\mathrm{GeV}$) energy fluxes[7] for the analyzed sample of Seyfert galaxies (denoted in the figure by black open circles), together with a corresponding luminosity-luminosity ($L_\gamma - L_\mathrm{X}$) plot in the right panel. We discuss the γ-ray results based on the LAT upper limits derived with an assumed photon index of 2.5. Dotted lines in the figures from top left to bottom right denote the ratios between the γ-ray and hard X-ray energy fluxes (or luminosities) $F_{0.1-10\,\mathrm{GeV}}/F_{14-195\,\mathrm{keV}} = 1$, 0.1, and 0.01, respectively. The distribution of the ratio between the γ-ray and hard X-ray luminosities is reported in Figure 4. As shown in the figure, for most of the analyzed objects the upper limits for this ratio are below 10 %, and for several particular sources are even below 1 %. The main conclusion here is that our investigation of the *Fermi*–LAT data indicate that there is no emission component around GeV photon energies in Seyfert objects down to the level of $L_\gamma/L_\mathrm{X} < 0.1$ in most cases.

It is instructive to locate intriguing targets from the sample in the parameter space of both panels of Figure 3, namely ESO 323–G077 and NGC 6814, the radio-intermediate quasar Mrk 1501, and the brightest hard-X-ray Seyfert galaxy in the sample NGC 4151. For comparison, two LAT-detected starburst galaxies showing Seyfert activity (NGC 1068 and NGC 4945) are plotted in the figure as well. The multifrequency data together with the *Fermi*–LAT fluxes for these are taken from Ackermann et al. (2011b, see also Table 3). As shown, although NGC 4151 is the brightest hard X-ray source among the analyzed Seyfert

[7] Upper limits of the energy fluxes (and corresponding luminosities) are calculated with the upper energy bound of 10 GeV based on the integrated photon flux upper limits above 0.1 GeV.

galaxies, its intrinsic hard X-ray luminosity is relatively modest, $L_{\rm X} \sim 10^{43}\,{\rm erg\,s^{-1}}$. Importantly, the γ-ray–to–hard X-ray luminosity ratio for this Seyfert is the lowest among our sample, $L_{\gamma}/L_{\rm X} \sim 0.0025$. This can be compared with ESO 323–G077 and NGC 6814, for which the X-ray luminosities in the BAT range are comparable to that of NGC 4151, but for which the luminosity ratios would be $L_{\gamma}/L_{\rm X} \sim 0.11$ and 0.093 in the case of the associations with 2FGL J1306.9–4028 and 2FGL J1942.5–1024, respectively. Mrk 1501 is yet a different case, being characterized by a relatively low X-ray flux but high X-ray luminosity, $L_{\rm X} \gtrsim 10^{44}\,{\rm erg\,s^{-1}}$. Indeed, this is the most distant object in the compiled sample. The two starburst galaxies included here for comparison, NGC 4945 and NGC 1068, are characterized by low hard X-ray luminosities, $L_{\rm X} \sim 10^{42}\,{\rm erg\,s^{-1}}$, and γ-ray–to–hard X-ray luminosity ratios $L_{\gamma}/L_{\rm X} \sim 0.1$.

Fermi–LAT upper limits derived for the analyzed Seyferts can be also compared with infrared fluxes measured by the *AKARI* satellite. Here we use *AKARI* 9 μm data (Ishihara et al. 2010) and 90 μm data (Yamamura et al. 2010) with a 'good' quality ($FQUAL = 3$), which are available for 65 and 73 sources from the analyzed sample, respectively. In the left and right panels of Figure 5 we present the corresponding luminosity-luminosity plots, including for comparison, the LAT-detected starburst galaxies NGC 1068, NGC 4945, NGC 253 and M 82 utilizing the *Fermi*–LAT data analysis presented in Ackermann et al. (2011b, see also Table 3 below). However, *AKARI* 90 μm data for NGC 4945, NGC 253 and M 82 are flagged as 'bad' quality ($FQUAL = 1$). Hence, for these sources we use instead IRAS 60 μm data (Sanders et al. 2003), which can be considered as comparable to the *AKARI* 90 μm data according to Yamamura et al. (2010).

The far-infrared fluxes of Seyferts galaxies ('FIR'; 90 μm data) are expected to be dominated by thermal dust emission related to the star-forming activity of the galactic hosts, while mid-infrared fluxes ('MIR'; 9 μm data) may originate substantially from circumnuclear dust heated by accretion disk emission, i.e. AGN activity. For most of the analyzed Seyferts the upper limits for the $L_{\gamma}/L_{\rm FIR}$ and $L_{\gamma}/L_{\rm MIR}$ ratios are in the range $0.01 - 0.1$ (cf. black dotted lines in the plots). At the same time, the LAT-detected starburst galaxies are characterized by $L_{\gamma}/L_{\rm FIR} \lesssim 0.001$. This suggests that detection of ISM emission in the GeV photon energy range from the bulk of the hard X-ray selected Seyfert objects — emission analogous to that observed in nearby star-forming galaxies — would require increasing the sensitivity of the *Fermi*–LAT survey by roughly an order of magnitude. Yet, in the analyzed sample there are also some outliers with particularly high FIR luminosities and *Fermi*–LAT upper limits low enough to already probe the GeV fluxes close to the expected level of the ISM-related γ-ray emission.

A similar conclusion can be drawn from Figure 6, where we plot radio 1.4 GHz luminosi-

ties versus upper limits for the γ-ray luminosities derived for the analyzed Seyferts, including also the comparison sample of starburst galaxies. The thick dotted cyan line shown in the figure represents the best-fit power-law relation between the radio and GeV luminosities for star-forming and local galaxies discussed in Ackermann et al. (2011b). The upper limits for the ratio $L_\gamma/L_{\rm R}$ in Seyfert sources are on average more than an order of magnitude above the γ-ray–to–radio luminosity ratios characterizing nearby star-forming galaxies. However, the relation between GeV and radio fluxes may not be expected to follow the trend established in star-forming systems for Seyferts in which AGN jet activity could contribute a substantial fraction of the total observed radio flux. Kataoka et al. (2011) argued that the jet-related γ-ray emission of Seyfert galaxies is expected to be below the flux levels probed at present by *Fermi*–LAT, at least for the majority of sources, and that conclusion is consistent with the upper limits presented in this work: γ-ray–to–radio luminosity ratio $L_\gamma/L_{\rm R} < 10^4$, on average.

The issue of excess radio emission related to the jet activity in Seyfert galaxies may be addressed by looking at the ratio of FIR and radio luminosities for the considered targets, since a relatively tight FIR–radio correlation has been established for non-active (and therefore not jetted) galaxies (see, e.g., Yun et al. 2010). Seyferts with particularly low FIR–to–radio luminosity ratios are likely characterized by prominent jet activity. In Figure 7 we plot $L_{\rm FIR}/L_{\rm R}$ versus upper limits for the γ-ray luminosities for the analyzed sample. As expected, there are many hard X-ray–selected Seyferts which are characterized by much lower $L_{\rm FIR}/L_{\rm R}$ ratios than those in nearby starburst galaxies. For instance, NGC 4151, which has a relatively prominent pc-scale and kpc-scale jet (Mundell et al. 2003; Ulvestad et al. 2005), shows one of the lowest $L_{\rm FIR}/L_{\rm R}$ ratio among the samples. In the case of ESO 323–G077 and NGC 6814 — which are not characterized by any outstanding radio or infrared luminosity when compared with the other Seyferts included in the sample — the ratio of the FIR and radio luminosities is very similar to that observed in the LAT-detected starburst galaxies, implying that ESO 323–G077 and NGC 6814 obey the FIR-radio correlation well, and hence that there is not much room for jet activity in these sources. This is in agreement with a non-detection of a compact radio core in ESO 323–G077 by high-resolution VLBI radio observations (Corbett et al. 2003), and with the presence of only weak steep-spectrum radio core in NGC 6814 (Ulvestad & Wilson 1984).

5.2. Possible γ-ray Emission Components in Seyfert Galaxies

The *Fermi*–LAT upper limits derived for the Seyfert galaxies in our sample probe the γ-ray luminosity range $L_\gamma/L_{\rm X} < 0.1$, and even < 0.01 in some cases. Since hard X-ray

luminosity is expected to constitute about 10 % of the bolometric AGN-related luminosity of a typical Seyfert galaxy (see Ho 2008), the results indicate that there is no emission component in Seyfert spectra at GeV photon energies down to the level of 1 % of the bolometric AGN-related luminosity, or even 0.1 % for several objects. The results imposes important constraints on any model of high energy radiation produced by Seyfert-type AGN.

There are several scenarios discussed in the literature in this context. For example, as noted above, the star-forming activity taking place in the host galaxies of Seyfert objects should result in non-negligible production of γ rays in the ISM. This inevitable emission component in Seyfert spectra is expected to be analogous to that observed by *Fermi*–LAT in a few nearby star-forming galaxies (Ackermann et al. 2011b), and as such is expected to scale with the FIR and with the diffuse radio luminosities of the host galaxies. However, the flux level probed by the *Fermi*–LAT in three years of all-sky survey does not allow for the detection of such diffuse emission for the majority of Seyferts, with a possible exception for the most nearby and actively star-forming targets. Teng et al. (2011) also mentioned the lack of detection of more distant Seyfert galaxies is likely a *Fermi*–LAT sensitivity issue based on their results of stacking analysis of 215 undetected Seyfert objects. They derived the upper limit in the 1–100 GeV energy range from the stacking analysis to be $\sim 3 \times 10^{41} \mathrm{erg\,s^{-1}}$ assuming the median redshift of the 215 stacked objects ($z \sim 0.031$), but it is still approximately 3 and 18 times the γ-ray luminosities at 1–100 GeV of NGC 1068 and NGC 4945, respectively.

In the previous section, we also commented on a possible contribution of radio jets to the γ-ray emission of Seyfert sources. Unlike the ISM-related γ-ray output, this jet-related emission component in Seyfert spectra at GeV photon energies is a subject of speculation (see, e.g., Lenain et al. 2010; Kataoka et al. 2011). Four AGN classified as NLS1s have been recently detected by *Fermi*–LAT and their observed high-energy radiation was established to be due to the jet activity (Abdo et al. 2009b; Foschini et al. 2011b). Those objects are however very different systems from the ones analyzed in this work, possessing flat-spectrum and high-brightness temperature radio cores, and therefore relativistic compact jets resembling blazar sources rather than sub-relativistic outflows observed in radio-quiet Seyferts (e.g., Foschini et al. 2009). Since the targets studied in this paper should be considered as being representative for the whole population of such ‘classical’ Seyferts, our analysis indicates that any jet-related γ-ray emission component in this type of AGN, even if present, is not as prominent as in radio galaxies or blazars.

Another possible emission site of γ-rays in Seyfert galaxies could be disk coronae, where the bulk of observed hard X-ray emission from Seyferts is produced. The first models for such emission involved non-thermal electron populations, and predicted power-law tails in

Seyfert spectra extending to at least MeV photon energies (e.g. Zdziarski & Lightman 1985; Svensson 1987). However, detections of spectral cut-offs in the hard X-ray continua around a few hundred keV photon energies in Seyfert galaxies favor emission models involving dominant thermal electron populations (see the discussion in Poutanen 1998; Zdziarski 1999). Still, the available observational constraints do not exclude the presence of non-thermal power-law tails in Seyfert spectra in the MeV range, albeit with a much reduced normalization, constituting not more than $\sim 10\,\%$ of total energy radiated in the X-ray regime (Johnson et al. 1997; Wardziński & Zdziarski 2001; Lubiński et al. 2010). Under this assumption, the observationally allowed luminosity ratio between the MeV ($0.1-10\,\mathrm{MeV}$) and the X-ray bands, $L_{0.1-10\,\mathrm{MeV}}/L_{\mathrm{X}} < 0.1$, together with a simple scaling of the $0.1-10\,\mathrm{GeV}$ luminosity $L_{\gamma} = 10^{3\,(2-\Gamma)}\,L_{0.1-10\,\mathrm{MeV}}$, formally implies an expected ratio $L_{\gamma}/L_{\mathrm{X}} < 0.003$ for $\Gamma = 2.5$. The current *Fermi*–LAT sensitivity can hardly probe such levels of γ-ray emission at the moment. In addition, even if the high energy emission were to originate in or near the accretion disk, the opacity of γ rays to pair production via interaction with X-rays produced by the accretion disk might prevent those γ rays from escaping. Nevertheless, as pointed out by Inoue et al. (2008), presence of such an emission component at the maximum allowed level would explain the observed extragalactic MeV background radiation in terms of a dominant contribution from Seyfert galaxies while Teng et al. (2011) suggest the radio-quiet Seyfert galaxies are not a significant source of the extragalactic γ-ray background above 1 GeV based on their analysis results of no γ-ray detection from the radio-quiet Seyfert galaxies at that energy range.

Finally, we discuss a possible mechanism of producing GeV photon in Seyfert galaxies by proton-proton interactions in the innermost parts of their accretion disks. Such a possibility was discussed previously in the context of Galactic black hole systems (Shapiro et al. 1976; Mahadevan et al. 1997; Oka & Manmoto 2003), and was applied recently to the case of active galaxies by Niedzwiecki et al. (2009). Although the current model predictions are still preliminary, this hadronic process was anticipated to result in a significant emission component in the $0.1-10\,\mathrm{GeV}$ range, possibly constituting $\gtrsim 10\,\%$ of the disk/disk corona X-ray luminosity in the case of a particular (preferred) range of the accretion rate, typically corresponding to advection-dominated ("hot") accretion flow, and of a maximally spinning black hole. That is because for a Kerr black hole the innermost stable orbit of the accretion disk can be located much closer to the event horizon, and hence the number density of the matter within the innermost parts of the accretion disk as well as the proton temperature are increased, leading to enhanced proton-proton interactions above the threshold for the pion production. The *Fermi*–LAT upper limits derived in this work for the sample of the hard X-ray–brightest Seyfert objects (mostly $L_{\gamma}/L_{\mathrm{X}} < 0.1$, and < 0.01 in several particular cases) could be useful to constrain the model parameters and, ultimately, to determine the spin

distribution for supermassive black holes hosted by Seyfert-type AGN. In this context, we find no prominent GeV emission component that could be related to hadronic interactions within accretion flows surrounding Kerr black holes for the whole analyzed sample, with the possible exceptions of ESO 323–G077 and NGC 6814.

As emphasized above, we cannot rule out the possibility that the associations of 2FGL J1306.9–4028 with ESO 323–G077 and 2FGL J1942.5–1024 with NGC 6814 are due to chance spatial coincidences, but if the Seyfert objects are conclusively established as γ-ray emitters, then neither the star-forming nor the jet activity in these objects can be considered as origins of the γ-ray emission. Figure 8 shows the broad-band spectral energy distribution of ESO 323–G077 (red data points), including the *Fermi*–LAT spectrum of 2FGL J1306.9–4028 (magenta data points), as well as NGC 6814 (dark green data points), and 2FGL J1942.5–1024 (green data points). For comparison, in the figure we also plot the broad-band spectral energy distribution of the starburst galaxy NGC 1068 (blue data points). As shown in the figure and discussed in the previous section, the γ-ray–to–far-infrared luminosity ratio for ESO 323–G077/2FGL J1306.9–4028 is much larger than for NGC 1068, which seems to exclude the possibility that the γ-ray emission from ESO 323–G077/2FGL J1306.9–4028 is attributed to the star-forming activity within the host of the analyzed Seyfert. On one hand, no compact radio core is found in ESO 323–G077 even by high-resolution ($< 0''.05$) VLBI observations, and the resultant upper limit for the radio core emission is 1.3 mJy at 2.3 GHz (Corbett et al. 2002, 2003). This finding challenges the jet hypothesis for the origin of γ rays, if ESO 323–G077 is associated with 2FGL J1306.9–4028. Therefore, either the association of 2FGL J1306.9–4028 with ESO 323–G077 is due to a chance positional coincidence, or ESO 323–G077 is an exceptional source for which the γ-ray radiative output is dominated by an emission component not typically observed among other Seyferts. The same reasoning may be applied in the case of NGC 6814.

6. Conclusion

In this paper, we report on a search for γ-ray emission from a sample of Seyfert galaxies selected via their hard X-ray fluxes, specifically for sources with $14 - 195$ keV fluxes above 2.5×10^{-11} erg cm^{-2} s^{-1} as determined using the *Swift*–BAT 58-month catalog, utilizing the three-year accumulation of *Fermi*–LAT data. We exclude 'radio-loud' objects from the sample by selecting only those sources for which the parameter R_{rX} — the ratio of νF_ν radio flux at 1.4 GHz frequency to the hard X-ray flux in the $14 - 195$ keV band — is less than 10^{-4}. The selection criteria leave us with a well-defined sample of 120 'radio-quiet' Seyfert galaxies. The two nearby type-2 Seyferts which *are* detected by the *Fermi*–LAT, NGC 1068

and NGC 4945, are not included in the analysis. In a companion paper by Ackermann et al. (2011b), we argue that the γ-ray emission of those two sources is more likely attributed to cosmic-ray interactions in the ISM of their host galaxies.

Generally, 'radio-quiet' Seyfert galaxies selected by their hard X-ray flux are *not* detected in the γ-ray band covered by the *Fermi*–LAT . We report photon flux upper limits for all the sources included in our sample: the typical limit is $\sim 4 \times 10^{-9}$ photons cm^{-2} s^{-1} in the energy range above 100 MeV. We find two possible associations of γ-ray sources with objects in our sample, ESO 323–G077 and NGC 6814, but caution that chance spatial coincidences with these objects cannot be ruled out.

FIR fluxes of the objects considered here, provided by the *AKARI* satellite, indicate the upper limits for the $L_\gamma/L_{\rm FIR}$ luminosity ratios in the range of $0.01 - 0.1$. At the same time, the LAT-detected starburst galaxies are characterized by $L_\gamma/L_{\rm FIR} \lesssim 0.001$. This suggests that detection of ISM emission in the GeV photon energy range from bulk of the hard X-ray selected Seyfert objects — emission analogous to that observed in nearby star-forming galaxies — would require increasing the sensitivity of the *Fermi*–LAT survey by roughly an order of magnitude. Similarly, the derived upper limits for the γ-ray-to-radio luminosity ratio, $L_\gamma/L_{\rm R} < 10^4$ on average, supports the conclusion by Kataoka et al. (2011) that the jet-related γ-ray emission of Seyfert galaxies is generally expected to be below the flux levels probed at present by *Fermi*–LAT .

The resultant *Fermi*–LAT upper limits yield the ratio of γ-ray to X-ray luminosities $L_\gamma/L_{\rm X} < 0.1$, and even < 0.01 in some cases. In general, coronae of accretion disks including non-thermal electron populations can be considered as plausible sites of the γ-ray production. Our analysis allows for the presence of such a broad-band power-law emission component extending from MeV to GeV range, but constituting not more than 10 % of the thermal radiative output of the disks and disk coronae.

Finally, γ-ray photons may be produced in Seyfert galaxies by proton-proton interactions in the innermost parts of their accretion disks. Although the current model predictions are still preliminary, this hadronic process was anticipated to result in a significant emission component in the $0.1 - 10$ GeV range, possibly constituting $\gtrsim 10$ % of the disk/disk corona X-ray luminosity in the case of a maximally spinning black hole. The upper limits derived in this paper indicate that no prominent GeV emission component that could be related to the hadronic interactions within accretion flows is found for the whole analyzed sample, with the possible exceptions of ESO 323–G077 and NGC 6814.

The *Fermi*–LAT Collaboration acknowledges generous ongoing support from a number of agencies and institutes that have supported both the development and the operation of the

LAT as well as scientific data analysis. These include the National Aeronautics and Space Administration and the Department of Energy in the United States, the Commissariat à l'Energie Atomique and the Centre National de la Recherche Scientifique / Institut National de Physique Nucléaire et de Physique des Particules in France, the Agenzia Spaziale Italiana and the Istituto Nazionale di Fisica Nucleare in Italy, the Ministry of Education, Culture, Sports, Science and Technology (MEXT), High Energy Accelerator Research Organization (KEK) and Japan Aerospace Exploration Agency (JAXA) in Japan, and the K. A. Wallenberg Foundation, the Swedish Research Council and the Swedish National Space Board in Sweden. Additional support for science analysis during the operations phase is gratefully acknowledged from the Istituto Nazionale di Astrofisica in Italy and the Centre National d'Études Spatiales in France.

This research has made use of the NASA/IPAC Extragalactic Database (NED) which is operated by the Jet Propulsion Laboratory, California Institute of Technology, under contract with the National Aeronautics and Space Administration.

M. H. is supported by the Research Fellowships of the Japan Society for the Promotion of Science for Young Scientists. K. B. is supported by a Stanford Graduate Fellowship. We thank the anonymous referee for the valuable comments that helped to improve the paper.

Facilities: Fermi–LAT , *Swift*–BAT , *AKARI*

REFERENCES

Abdo, A. A., et al. 2009a, Astroparticle Physics, 32, 193

Abdo, A. A., et al. 2009b, ApJ, 707, L142

Abdo, A. A., et al. 2010a, ApJ, 715, 429

Abdo, A. A., et al. 2010b, ApJS, 188, 405

Abdo, A. A., et al. 2010c, ApJ, 720, 912

Abdo, A. A., et al. 2011, submitted to ApJS, arXiv:1108.1435

Ackermann, M., et al. 2011a, ApJ, 743, 171

Ackermann, M., et al. 2011b, submitted to ApJ

Ajello, M., et al. 2008, ApJ, 673, 96

Antonucci, R. 1993, ARA&A, 31, 473

Atwood, W., et al. 2009 ApJ, 697, 1071

Barthelmy, S. D., et al. 2005, Space Sci. Rev., 120, 143

Baumgartner, W. H., et al. 2010, submitted to ApJS, http://heasarc.gsfc.nasa.gov/docs/swift/results/bs58mon/

Becker, R. H., Helfand, D. J., White, R. L., Gregg, M. D., & Laurent-Muehleisen, S. A. 2003, VizieR Online Data Catalog, 8071, 0

Beckmann, V., et al. 2009, A&A, 505, 417

Bignami, G. F., Fichtel, C. E., Hartman, R. C., & Thompson, D. J. 1979, ApJ, 232, 649

Brunthaler, A., et al. 2000, A&A, 357, L45

Burlon, D., Ajello, M., Greiner, J., Comastri, A., Merloni, A., & Gehrels, N. 2011, ApJ, 728, 58

Cappi, M., et al. 2006, A&A, 446, 459

Cillis, A. N., Hartman, R. C., & Bertsch, D. L. 2004, ApJ, 601, 142

Condon, J. J., Helou, G., Sanders, D. B., & Soifer, B. T. 1996, ApJS, 103, 81

Condon, J. J., Cotton, W. D., Greisen, E. W., Yin, Q. F., Perley, R. A., Taylor, G. B., & Broderick, J. J. 1998, AJ, 115, 1693

Corbett, E. A., et al. 2002, ApJ, 564, 650

Corbett, E. A., et al. 2003, ApJ, 583, 670

Cusumano, G., et al. 2010, A&A, 524, A64

Foschini, L., Maraschi, L., Tavecchio, F., Ghisellini, G., Gliozzi, M., & Sambruna, R. M. 2009, Advances in Space Research, 43, 889

Foschini L., Colpi M., Gallo L., et al. (eds), 2011a, Narrow-Line Seyfert 1 Galaxies and Their Place in the Universe, Proceedings of Science, vol. NLS1, (Trieste: PoS/SISSA), http://pos.sissa.it/cgi-bin/reader/conf.cgi?confid=126

Foschini, L., Ghisellini, G., Kovalev, Y. Y., et al. 2011b, MNRAS, 413, 1671

Gallimore, J. F., Axon, D. J., O'Dea, C. P., Baum, S. A., & Pedlar, A. 2006, AJ, 132, 546

Gilli, R., Comastri, A., & Hasinger, G. 2007, A&A, 463, 79

Gondek, D., Zdziarski, A. A., Johnson, W. N., George, I. M., McNaron-Brown, K., Magdziarz, P., Smith, D., & Gruber, D. E. 1996, MNRAS, 282, 646

Healey, S. E., Romani, R. W., Taylor, G. B., Sadler, E. M., Ricci, R., Murphy, T., Ulvestad, J. S., & Winn, J. N. 2007, ApJS, 171, 61

Helene, O. 1983, Nuclear Instruments and Methods in Physics Research, 212, 319

Ho, L. C. 2002, ApJ, 564, 120

Ho, L. C. 2008, ARA&A, 46, 475

Ho, L. C., & Peng, C. Y. 2001, ApJ, 555, 650

Ho, L. C., & Ulvestad, J. S. 2001, ApJS, 133, 77

Ho, L. C., et al. 2001, ApJ, 549, L51

Inoue, Y., Totani, T., & Ueda, Y. 2008, ApJ, 672, L5

Ishihara, D., et al. 2010, A&A, 514, A1

Johnson, W. N., McNaron-Brown, K., Kurfess, J. D., Zdziarski, A. A., Magdziarz, P., & Gehrels, N. 1997, ApJ, 482, 173

Kataoka, J., et al. 2011, ApJ, 740, 29

Kellermann, K. I., et al. 1989, AJ, 98, 1195

Kukula, M. J., Pedlar, A., Baum, S. A., & O'Dea, C. P. 1995, MNRAS, 276, 1262

Lal, D. V., Shastri, P., & Gabuzda, D. C. 2011, ApJ, 731, 68

Lenain, J.-P., Ricci, C., Türler, M., Dorner, D., & Walter, R. 2010, A&A, 524, A72

Lin, Y. C., et al. 1993, ApJ, 416, L53

Lodato, G., & Bertin, G. 2003, A&A, 398, 517

Lubiński, P., Zdziarski, A. A., Walter, R., Paltani, S., Beckmann, V., Soldi, S., Ferrigno, C., & Courvoisier, T. J.-L. 2010, MNRAS, 408, 1851

Mahadevan, R., Narayan, R., & Krolik, J. 1997, ApJ, 486, 268

Maisack, M., et al. 1995, A&A, 298, 400

Maisack, M., Mannheim, K., & Collmar, W. 1997, A&A, 319, 397

Massaro, E., et al. 2009, A&A, 495, 691

Mattox, J. R., et al. 1996, ApJ, 461, 396

Mauch, T., Murphy, T., Buttery, H. J., Curran, J., Hunstead, R. W., Piestrzynski, B., Ropbertson, J. G., & Sadler, E. M. 2008, VizieR Online Data Catalog, 8081, 0

McConville, W., et al. 2011, ApJ, 738, 148

Middelberg, E., et al. 2004, A&A, 417, 925

Miller, P., Rawlings, S., & Saunders, R. 1993, MNRAS, 263, 425

Mundell, C. G., Wrobel, J. M., Pedlar, A., & Gallimore, J. F. 2003, ApJ, 583, 192

Niedzwiecki, A., Xie, F. G., & Zdziarski, A. A. 2009, The Extreme Sky: Sampling the Universe above 10 keV,

Oka, K., & Manmoto, T. 2003, MNRAS, 340, 543

Osterbrock, D. E. 1977, ApJ, 215, 733

Osterbrock, D. E. 1989, Astrophysics of Gaseous Nebulae and Active Galactic Nuclei, (Mill Valley: University Science Books)

Panessa, F., Barcons, X., Bassani, L., Cappi, M., Carrera, F. J., Ho, L. C., & Pellegrini, S. 2007, A&A, 467, 519

Pogge, R. W. 2000, New A Rev., 44, 381

Pollock, A. M. T., Masnou, J. L., Bignami, G. F., Hermsen, W., Swanenburg, B. N., Kanbach, G., Lichti, G. G., & Wills, R. D. 1981, A&A, 94, 116

Poutanen, J. 1998, Theory of Black Hole Accretion Disks, 100

Sanders, D. B., Mazzarella, J. M., Kim, D.-C., Surace, J. A., & Soifer, B. T. 2003, AJ, 126, 1607

Schoenfelder, V., et al. 1993, ApJS, 86, 657

Seyfert, C. K. 1943, ApJ, 97, 28

Shapiro, S. L., Lightman, A. P., & Eardley, D. M. 1976, ApJ, 204, 187

Sikora, M., Stawarz, Ł., & Lasota, J. P. 2007, ApJ, 658, 815

Svensson, R. 1987, MNRAS, 227, 403

Teng, S. H., Mushotzky, R. F., Sambruna, R. M., Davis, D. S., & Reynolds, C. S. 2011, ApJ, 742, 66

Terashima, Y., & Wilson, A. S. 2003, ApJ, 583, 145

Thompson, D. J., et al. 1993, ApJS, 86, 629

Tueller, J., Mushotzky, R. F., Barthelmy, S., Cannizzo, J. K., Gehrels, N., Markwardt, C. B., Skinner, G. K., & Winter, L. M. 2008, ApJ, 681, 113

Ulvestad, J. S., & Wilson, A. S. 1984, ApJ, 285, 439

Ulvestad, J. S., & Wilson, A. S. 1989, ApJ, 343, 659

Ulvestad, J. S., & Ho, L. C. 2001, ApJ, 558, 561

Ulvestad, J. S., Wong, D. S., Taylor, G. B., Gallimore, J. F., & Mundell, C. G. 2005, AJ, 130, 936

Wardziński, G., & Zdziarski, A. A. 2001, MNRAS, 325, 963

White, R. L., & Becker, R. H. 1992, ApJS, 79, 331

Wright, A., & Otrupcek, R. 1990, PKS Catalog (1990), 0

Yamamura, I., Makiuti, S., Ikeda, N., Fukuda, Y., Oyabu, S., Koga, T., & White, G. J. 2010, VizieR Online Data Catalog, 2298, 0

Yun, M. S., Reddy, N. A., & Condon, J. J. 2001, ApJ, 554, 803

Zdziarski, A. A. 1999, High Energy Processes in Accreting Black Holes, 161, 16

Zdziarski, A. A., & Lightman, A. P. 1985, ApJ, 294, L79

Zdziarski, A. A., Poutanen, J., & Johnson, W. N. 2000, ApJ, 542, 703

Zhou, X.-L., & Zhang, S.-N. 2010, ApJ, 713, L11

This preprint was prepared with the AAS LaTeX macros v5.2.

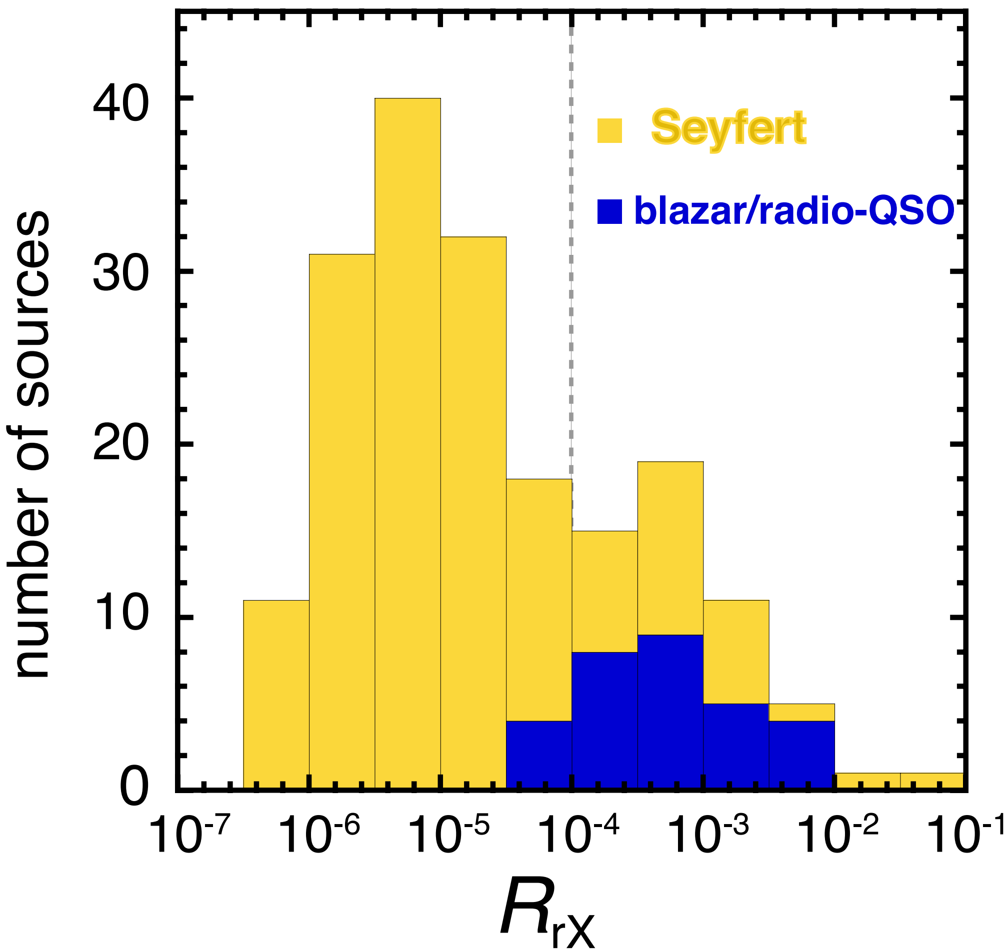

Fig. 1.— Distribution of the 'hard X-ray radio loudness parameter' $R_{\rm rX}$ for Seyfert galaxies selected from the *Swift*–BAT 58-month catalog based on the flux and position cuts described in § 2 (yellow bars), and also for the comparison sample of blazars and radio quasars (blue bars).

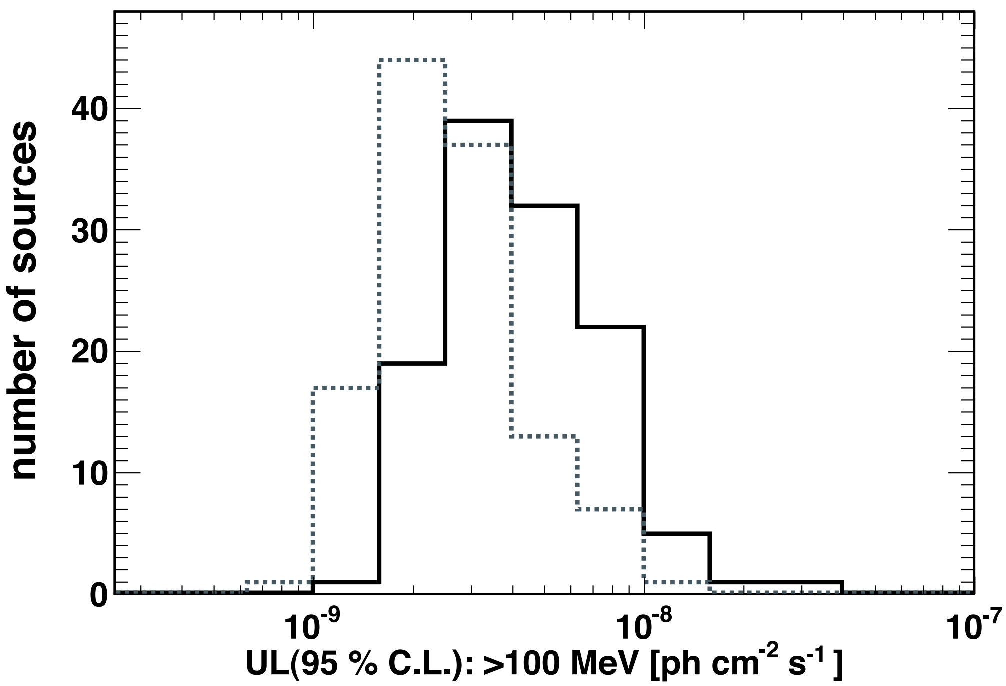

Fig. 2.— Distribution of the *Fermi*–LAT photon flux upper limits (95 % C.L.) for the analyzed sample of Seyfert galaxies calculated, assuming photon indices $\Gamma = 2.5$ (solid line) and $\Gamma = 2.2$ (dotted line) .

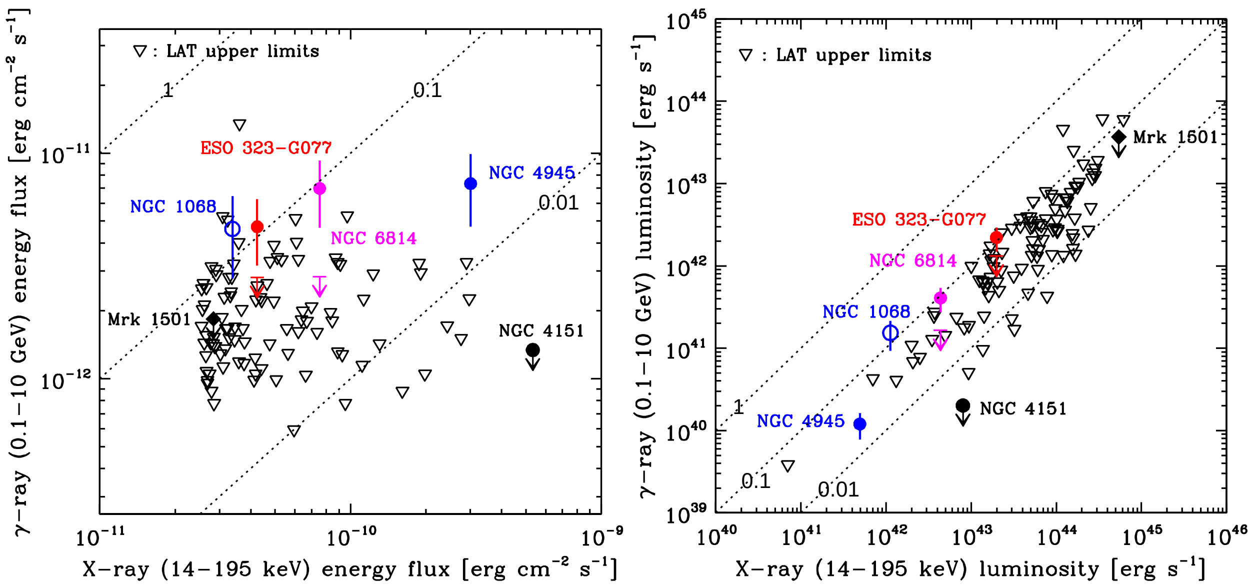

Fig. 3.— *Left:* Hard X-ray ($14-195\,\mathrm{keV}$) energy fluxes versus upper limits for the γ-ray ($0.1-10\,\mathrm{GeV}$) energy fluxes for the analyzed sample of Seyferts (denoted by black open triangles) assuming a photon index $\Gamma = 2.5$. Dotted lines from top left to bottom right denote the ratios between the γ-ray and hard X-ray energy fluxes 1, 0.1, and 0.01, respectively. Arrows denote ESO 323–G077 (red) and NGC 6814 (magenta) when the *Fermi*–LAT upper limit is considered, and each flux is denoted by a filled circle when assuming the associations with 2FGL J1306.9–4028 and 2FGL J1942.5–1024, respectively. The radio-intermediate quasar Mrk 1501 is denoted by a black filled diamond. NGC 4151 is marked by a black filled circle. For comparison, starburst galaxies NGC 1068 (blue open circle) and NGC 4945 (blue filled circle) are included. *Right:* The corresponding luminosity-luminosity plot.

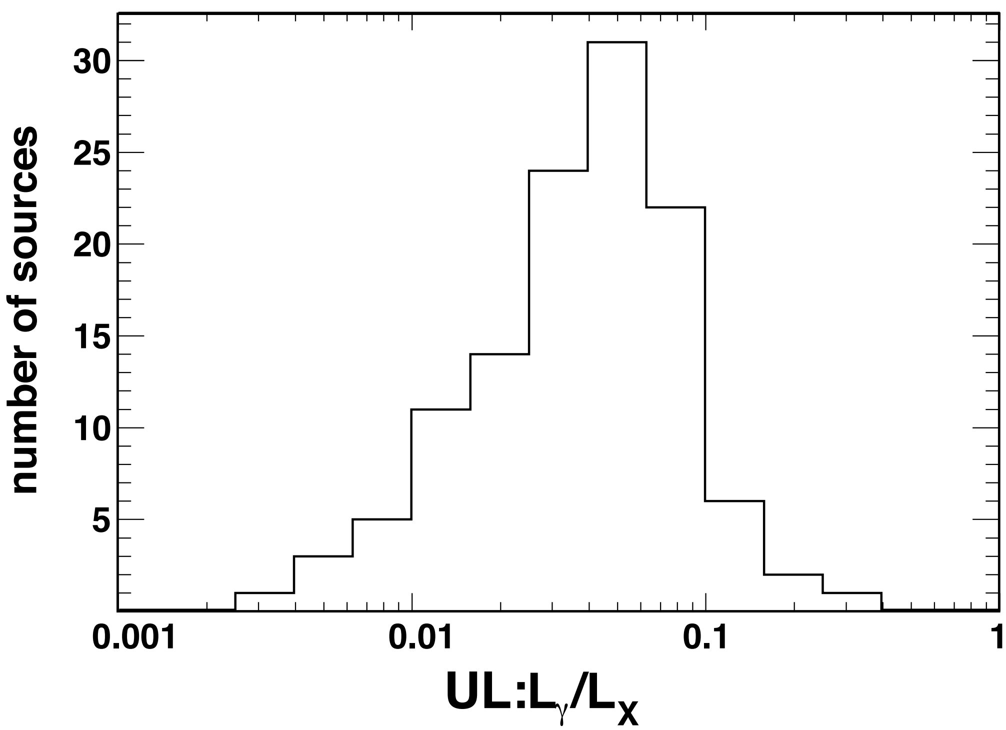

Fig. 4.— Distribution of γ-ray-to-hard X-ray luminosity ratio for the analyzed sample of Seyfert galaxies, based on the γ-ray upper limit with an assumed photon index $\Gamma = 2.5$.

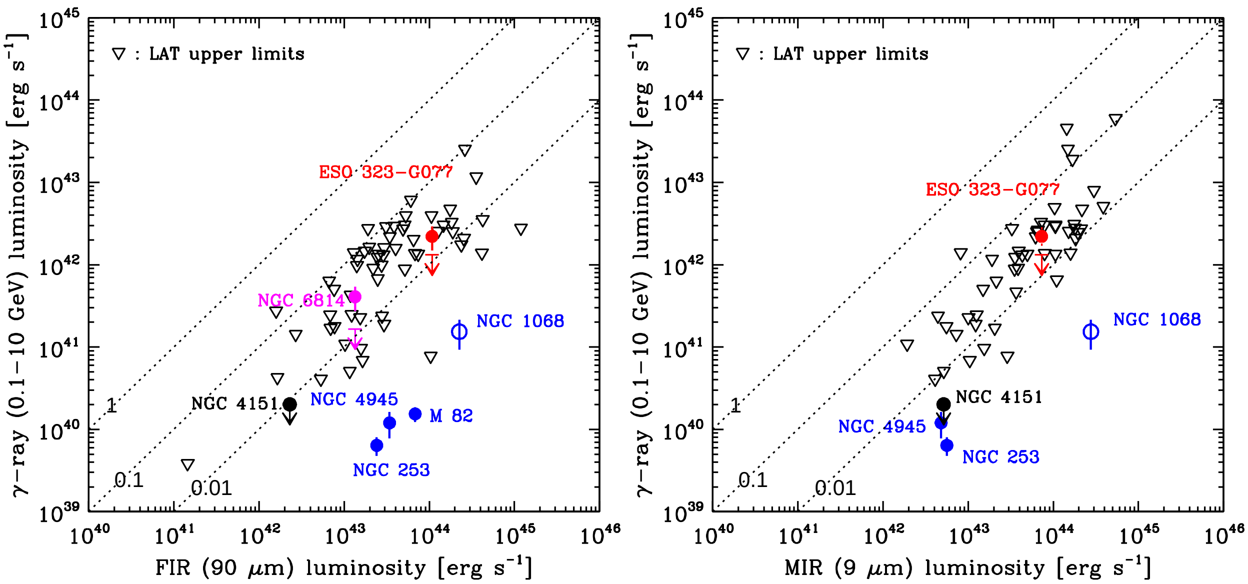

Fig. 5.— Far-infrared (90 μm; *left panel*) and mid-infrared (9 μm; *right panel*) luminosities versus upper limits for the γ-ray (0.1 − 10 GeV) luminosities for the analyzed sample of Seyferts assuming an photon index $\Gamma = 2.5$. Dotted lines from top left to bottom right denote the ratios between the γ-ray and infrared luminosities 1, 0.1, and 0.01, respectively. Arrows denote ESO 323–G077 (red) and NGC 6814 (magenta) when the *Fermi*–LAT upper limit is considered, and each flux is denoted by a filled circle when assuming the associations with 2FGL J1306.9–4028 and 2FGL J1942.5–1024, respectively. No *AKARI* 9 μm flux is available for NGC 6814. NGC 4151 is marked by black filled circle. For comparison, starburst galaxies NGC 1068 (blue open circles), NGC 4945, NGC 253 and M 82 (blue filled circles) are included.

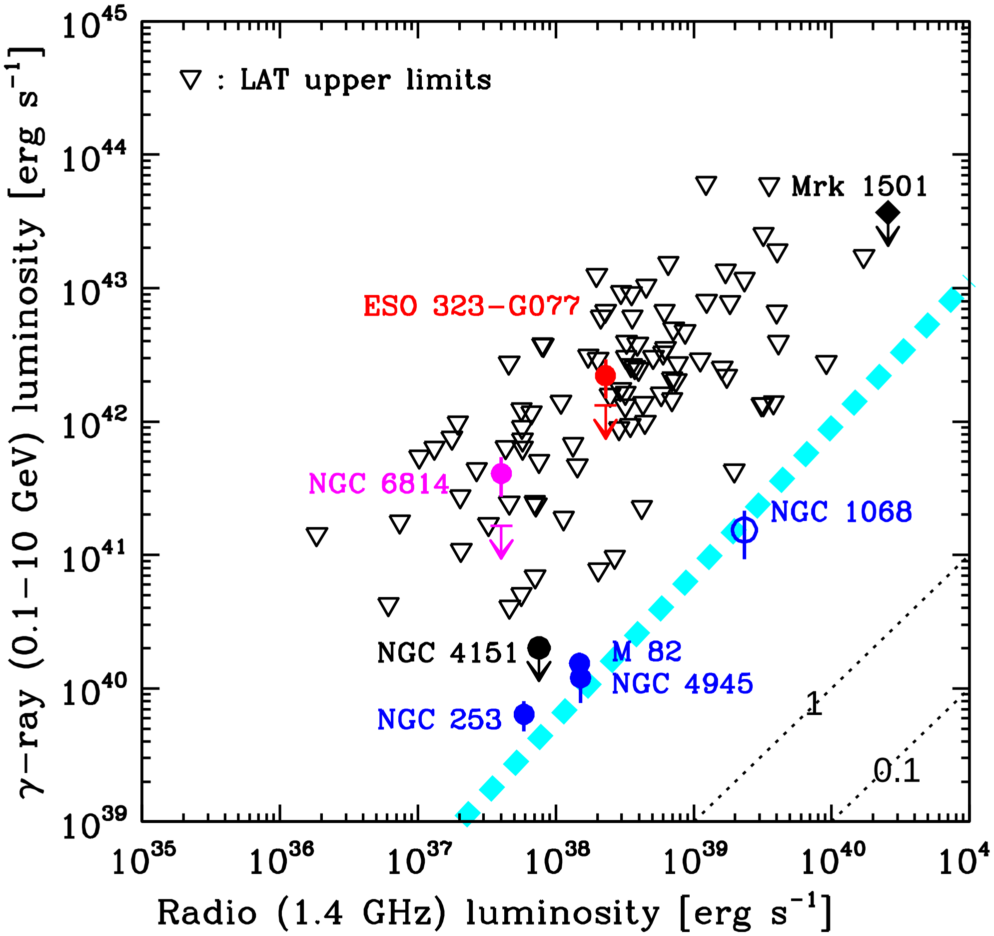

Fig. 6.— Radio (1.4 GHz) luminosities versus upper limits for the γ-ray $(0.1 - 10\,\mathrm{GeV})$ luminosities for the analyzed sample of Seyferts assuming a photon index $\Gamma = 2.5$. Black dotted lines from top left to bottom right denote the ratios between the γ-ray and radio luminosities 1 and 0.1, respectively. Arrows denote ESO 323–G077 (red) and NGC 6814 (magenta) when the *Fermi*–LAT upper limit is considered, and each flux is denoted by a filled circle when assuming the associations with 2FGL J1306.9–4028 and 2FGL J1942.5–1024, respectively. The radio-intermediate quasar Mrk 1501 is denoted by a black filled diamond. NGC 4151 is marked by a black filled circle. For comparison, starburst galaxies NGC 1068 (blue open circle), NGC 4945, NGC 253 and M 82 (blue filled circles) are included. The thick dotted cyan line represents the best-fit power-law relation between the radio and GeV luminosities for star-forming and local galaxies discussed in Ackermann et al. (2011b).

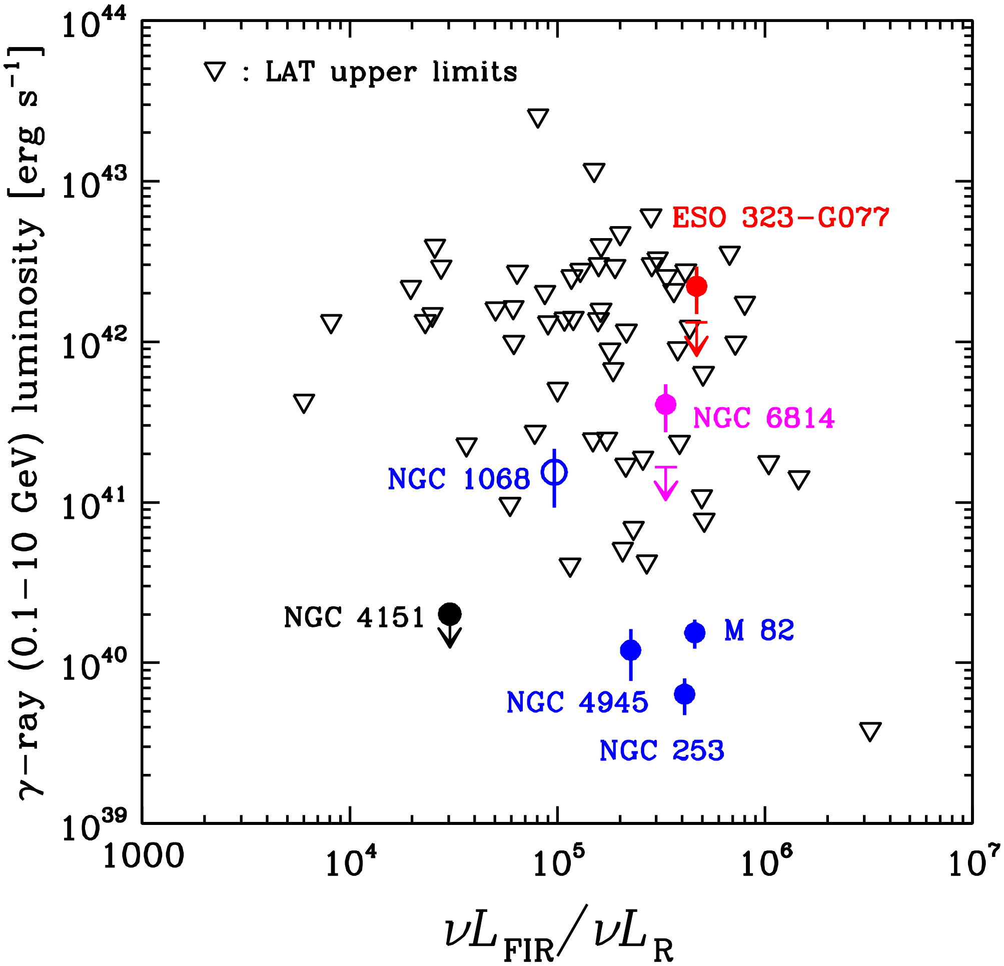

Fig. 7.— Far-infrared–to–radio luminosity ratios versus upper limits for the γ-ray (0.1 – 10 GeV) luminosities for the analyzed sample of Seyferts assuming a photon index Γ = 2.5. Arrows denote ESO 323–G077 (red) and NGC 6814 (magenta) when the *Fermi*–LAT upper limit is considered, and each flux is denoted by a filled circle when assuming the associations with 2FGL J1306.9–4028 and 2FGL J1942.5–1024, respectively. NGC 4151 is marked by a black filled circle. For comparison, starburst galaxies NGC 1068 (blue open circle), NGC 4945, NGC 253 and M 82 (blue filled circles) are included.

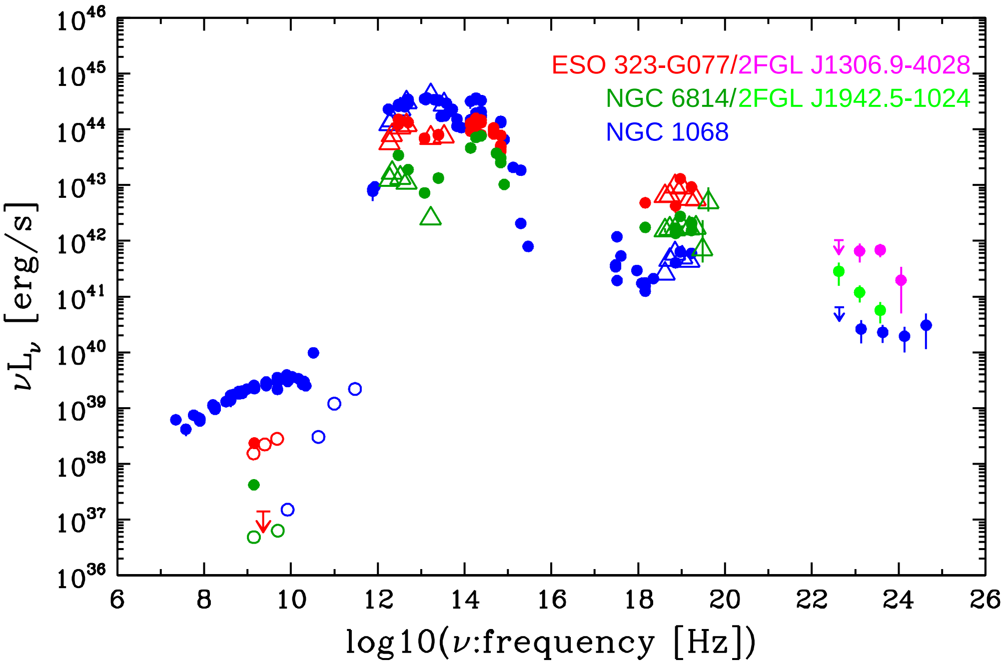

Fig. 8.— Broad-band spectral energy distributions of ESO 323–G077 (red) and NGC 6814 (dark green). Both *Fermi*–LAT spectra are derived when assuming the associations with 2FGL J1306.9–4028 (magenta) and 2FGL J1942.5–1024 (green), respectively. For comparison, broad-band spectral energy distribution of the starburst galaxy NGC 1068 (blue) is also shown including its *Fermi*–LAT data points from Ackermann et al. (2011b). The data are taken from NED (total flux: filled circle), *AKARI* and *Swift*–BAT (open triangle). In the radio regime, core fluxes are also denoted as open circles for ESO 323-G077 (from Corbett et al. 2002), for NGC 6814 (from Ulvestad & Wilson 1984) and for NGC 1068 (from NED). An upper limit for the radio compact core emission by high-resolution ($< 0''.05$) VLBI observations for ESO 323-G077 is also plotted (from Corbett et al. 2002).

Table 1. Basic information regarding Seyfert galaxies included in the analyzed sample

Name	R.A. [degree]	Dec [degree]	z	$d_{\rm L}$ [Mpc]	$F_{14-195\,{\rm keV}}$ [10^{-11} cgs]	log $L_{\rm X}$ [erg s^{-1}]	log $L_{\rm R}$ [erg s^{-1}]	ref.	log $R_{\rm rX}$	log $L_{\rm FIR}$ [erg s^{-1}]	log $L_{\rm MIR}$ [erg s^{-1}]	type
(1)	(2)	(3)	(4)	(5)	(6)	(7)	(8)	(9)	(10)	(11)	(12)	(13)
Mrk 1501	2.6292	10.9749	0.08934	400	2.84	44.74	40.41	1	-4.33	···	···	Sy1.2
NGC 235A	10.7200	-23.5410	0.02223	94.1	4.78	43.70	38.79	1	-4.91	44.63	···	Sy1
Mrk 348	12.1964	31.9570	0.01503	63.5	16.10	43.89	39.29	1	-4.60	43.08	···	Sy2
Mrk 1148	12.9783	17.4329	0.064	280.3	3.03	44.45	38.30	8	-6.16	···	···	Sy1
Mrk 352	14.9720	31.8269	0.01486	62.7	2.89	43.13	···	···	···	···	44.04	Sy1
Mrk 1152	18.4587	-14.8456	0.05271	228.4	2.83	44.25	38.55	1	-5.70	···	···	Sy1.5
Fairall 9	20.9408	-58.8057	0.04702	205.3	5.05	44.41	···	···	···	···	44.59	Sy1
NGC 526A	20.9766	-35.0654	0.0191	80.9	5.95	43.67	38.15	1	-5.51	···	43.56	Sy1.5
ESO 297-018	24.6548	-40.0114	0.0252	107.5	6.99	43.98	39.05	1	-4.94	43.49	···	Sy2
NGC 788	30.2769	-6.8155	0.0136	56.3	8.31	43.50	37.25	2	-6.25	···	···	Sy2
Mrk 1018	31.5666	-0.2914	0.04244	181.5	3.24	44.11	38.36	1	-5.75	···	···	Sy1.5
NGC 931	37.0603	31.3117	0.01665	50.4	6.08	43.27	37.75	1	-5.52	43.39	43.55	Sy1.5
NGC 973	38.5838	32.5056	0.01619	60.5	2.85	43.10	38.12	1	-4.97	43.39	···	Sy2
NGC 985	38.6574	-8.7876	0.043	184.7	3.11	44.10	38.94	1	-5.17	44.24	44.34	Sy1
ESO 416-G002	38.8061	-29.6047	0.0592	257.6	2.61	44.32	40.23	1	-4.08	···	···	Sy1.9
ESO 198-024	39.5821	-52.1923	0.0455	197.7	2.87	44.13	39.60	7	-4.53	···	···	Sy1
2MASX J02485937+2630391	42.2472	26.5109	0.0579	252.4	3.45	44.42	39.37	1	-5.05	44.55	···	Sy2
MCG-02-08-014	43.0975	-8.5104	0.01675	69.6	2.66	43.19	37.76	1	-5.43	···	···	Sy2
NGC 1142	43.8008	-0.1836	0.02885	121.5	9.52	44.23	39.58	1	-4.65	44.62	44.20	Sy2
ESO 417-G006	44.0898	-32.1856	0.01629	68.5	2.86	43.21	37.42	1	-5.78	···	···	Sy2
NGC 1194	45.9546	-1.1037	0.0136	56.2	3.72	43.15	37.12	1	-6.03	42.82	43.33	Sy1
RX J0311.3-2046	47.8284	-20.7717	0.066	293.8	2.77	44.46	38.81	1	-5.64	···	···	Sy1.5
NGC 1365	53.4016	-36.1404	0.00546	18.0	6.45	42.40	38.31	1	-4.09	44.02	43.46	Sy1.8
ESO 548-G081	55.5155	-21.2444	0.01448	60.4	4.20	43.26	37.29	1	-5.97	43.15	···	Sy1
ESO 549-G049	60.6070	-18.0480	0.02629	111.1	2.57	43.58	38.71	1	-4.87	44.17	43.90	Sy2
UGC 03142	70.9450	28.9718	0.02166	91.7	4.95	43.70	38.51	1	-5.19	43.72	···	Sy1
2MASX J04440903+2813003	71.0376	28.2168	0.01127	47.7	6.03	43.22	38.04	1	-5.18	43.11	42.91	Sy2
MCG-01-13-025	72.9229	-3.8094	0.01589	66.7	3.17	43.23	37.76	1	-5.47	···	···	Sy1.2
CGCG 420-015	73.3573	4.0616	0.02939	124.8	2.66	43.69	38.30	1	-5.39	43.59	44.02	Sy2
2MASX J05054575-2351139	76.4405	-23.8539	0.03504	150.3	6.19	44.22	38.47	1	-5.75	···	···	Sy2
CGCG 468-002NED01	77.0820	17.3630	0.0175	73.9	2.59	43.23	38.47	1	-4.76	44.38	···	Sy2
IRAS 05078+1626	77.6896	16.4989	0.01788	75.5	8.88	43.78	37.76	1	-6.03	43.34	43.59	Sy1.5
2MASX J05151978+1854515	78.8324	18.9143	···	···	3.31	···	···	1	-5.28	···	···	Galaxy
Ark 120	79.0476	-0.1498	0.0323	139.7	6.63	44.19	38.60	1	-5.59	···	44.29	Sy1
ESO 362-18	79.8993	-32.6578	0.01245	53.0	5.11	43.23	37.82	1	-5.41	43.16	43.28	Sy1.5
2MASX J05442257+5907361	86.0941	59.1267	0.06597	292.9	2.65	44.43	39.23	1	-5.20	···	···	Sy1.9
NGC 2110	88.0474	-7.4562	0.00779	29.0	29.74	43.48	38.62	1	-4.85	43.19	43.00	Sy2
MCG+08-11-011	88.7234	46.4393	0.02048	88.3	13.05	44.09	39.50	1	-4.58	43.87	44.02	Sy1.5
2MASX J05580206-3820043	89.5083	-38.3346	0.03387	146.7	2.90	43.87	39.09	1	-4.78	···	44.48	Sy1
ESO 005-G004	91.4235	-86.6319	0.00623	22.0	3.59	42.32	37.85	7	-4.47	43.21	43.02	Sy2
ESO 121-IG028	95.9400	-60.9790	0.0403	177.8	2.69	44.01	···	···	···	···	···	Sy2
ESO 426-G002	95.9434	-32.2166	0.02243	97.1	2.66	43.48	···	···	···	···	···	Sy2
ESO 490-IG026	100.0487	-25.8954	0.0248	107.7	3.78	43.72	38.87	1	-4.85	43.81	···	Sy1.2
2MASX J06411806+3249313	100.3252	32.8254	0.047	205.2	3.67	44.27	38.66	1	-5.61	···	···	Sy2
Mrk 6	103.0511	74.4271	0.01881	83.0	6.20	43.71	39.49	1	-4.22	43.40	43.69	Sy1.5
Mrk 79	115.6367	49.8097	0.02219	97.3	4.64	43.72	38.51	1	-5.21	43.71	44.02	Sy1.2
2MASX J07595347+2323241	119.9728	23.3901	0.02918	127.7	3.19	43.79	38.78	1	-5.02	44.26	43.85	Sy2
IC 0486	120.0874	26.6135	0.02688	112.0	3.58	43.73	38.33	1	-5.40	43.78	···	Sy1
Mrk 1210	121.0244	5.1138	0.0135	60.3	5.31	43.36	38.84	1	-4.52	43.24	43.59	Sy2

Table 1—Continued

Name	R.A. [degree]	Dec [degree]	z	$d_{\rm L}$ [Mpc]	$F_{14-195\,\rm keV}$ [10^{-11} cgs]	$\log L_{\rm X}$ [erg s^{-1}]	$\log L_{\rm R}$ [erg s^{-1}]	ref.	$\log R_{\rm rX}$	$\log L_{\rm FIR}$ [erg s^{-1}]	$\log L_{\rm MIR}$ [erg s^{-1}]	type
(1)	(2)	(3)	(4)	(5)	(6)	(7)	(8)	(9)	(10)	(11)	(12)	(13)
Fairall 272	125.7546	-4.9349	0.02182	96.7	4.76	43.73	38.76	1	-4.96	43.47	···	Sy2
Mrk 704	139.6084	16.3053	0.02923	130.0	3.28	43.82	38.23	1	-5.59	···	44.24	Sy1.5
MCG-01-24-012	140.1927	-8.0561	0.01964	89.0	4.12	43.59	38.54	1	-5.05	···	···	Sy2
MCG+04-22-042	140.9292	22.9090	0.03235	143.6	4.18	44.01	38.55	1	-5.47	···	43.82	Sy1.2
Mrk 110	141.3036	52.2863	0.03529	156.0	5.63	44.21	38.59	1	-5.62	···	···	Sy1
MCG-05-23-016	146.9173	-30.9489	0.00849	36.8	19.80	43.51	37.51	1	-6.00	42.84	43.31	Sy2
NGC 3081	149.8731	-22.8263	0.00796	28.6	8.44	42.92	36.87	1	-6.05	42.89	42.74	Sy2
ESO 263-G013	152.4509	-42.8112	0.03329	150.9	3.34	43.96	38.79	7	-5.17	···	···	Sy2
NGC 3227	155.8774	19.8651	0.00386	26.4	11.28	42.97	38.06	1	-4.92	43.47	43.09	Sy1.5
NGC 3281	157.9670	-34.8537	0.01067	46.4	8.71	43.35	38.46	1	-4.89	43.71	43.55	Sy2
2MASS J10315431-1416514	157.9763	-14.2809	0.086	387.3	3.42	44.79	39.54	1	-5.24	···	44.73	Sy1
NGC 3393	162.0977	-25.1621	0.01251	57.4	2.55	43.00	38.65	1	-4.36	43.44	···	Sy2
Mrk 417	162.3789	22.9644	0.03276	147.4	3.36	43.94	···	···	···	···	···	Sy2
NGC 3516	166.6979	72.5686	0.00884	38.0	12.31	43.33	37.88	1	-5.45	42.88	43.18	Sy1.5
NGC 3783	174.7572	-37.7386	0.00973	25.1	18.77	43.15	37.66	1	-5.49	42.83	43.10	Sy1
UGC 06728	176.3168	79.6815	0.00652	32.9	2.68	42.54	···	···	···	···	···	Sy1.2
2MASX J11454045-1827149	176.4186	-18.4543	0.03295	150.7	4.95	44.13	38.55	1	-5.57	···	···	Sy1
NGC 4051	180.7901	44.5313	0.00233	17.1	3.76	42.12	37.66	1	-4.45	42.73	42.61	Sy1.5
ARK 347	181.1237	20.3162	0.02244	104.1	2.92	43.58	37.90	1	-5.68	···	···	Sy2
NGC 4138	182.3741	43.6853	0.00296	13.8	3.07	41.84	36.78	1	-5.06	42.21	···	Sy1.9
NGC 4151	182.6357	39.4057	0.00332	11.2	53.31	42.90	37.88	1	-5.03	42.36	42.71	Sy1.5
NGC 4235	184.2912	7.1916	0.00804	31.5	3.14	42.57	37.31	1	-5.27	42.20	···	Sy1
NGC 4388	186.4448	12.6621	0.00842	16.8	27.58	42.97	37.75	1	-5.22	43.07	42.71	Sy2
NGC 4395	186.4538	33.5468	0.00106	4.74	2.61	40.85	34.65	2	-6.19	41.16	···	Sy1.9
NGC 4507	188.9026	-39.9093	0.0118	62.4	19.04	43.95	38.63	1	-5.31	43.83	43.90	Sy2
ESO 506-G027	189.7275	-27.3078	0.02502	119.0	9.26	44.20	39.24	1	-4.96	43.54	43.79	Sy2
LEDA 170194	189.7762	-16.1797	0.03667	167.7	4.37	44.17	39.26	1	-4.90	···	···	Sy2
NGC 4593	189.9143	-5.3443	0.009	37.3	8.87	43.17	37.01	1	-6.16	···	···	Sy1
NGC 4686	191.6661	54.5342	0.01674	77.8	2.79	43.31	37.64	1	-5.67	···	···	Galaxy
SBS 1301+540	195.9978	53.7917	0.02988	134.8	3.46	43.88	37.91	1	-5.96	···	···	Sy1
NGC 4939	196.0600	-10.3396	0.01037	34.7	2.54	42.56	37.85	1	-4.72	43.09	···	Sy2
ESO 323-G077	196.6089	-40.4146	0.01501	62.4	4.25	43.30	38.36	4	-4.94	44.03	43.86	Sy1.2
NGC 4992	197.2733	11.6341	0.02514	117.0	5.56	43.96	37.66	2	-6.30	43.28	43.52	Sy2
MCG-06-30-015	203.9741	-34.2956	0.00775	25.5	6.36	42.69	36.27	5	-6.43	42.43	42.86	Sy1.2
NGC 5252	204.5665	4.5426	0.02297	108.4	11.11	44.19	38.50	1	-5.69	43.29	···	Sy1.9
IC 4329A	207.3303	-30.3094	0.01605	83.0	28.96	44.38	38.88	1	-5.50	43.69	44.33	Sy1.2
Mrk 279	208.2644	69.3082	0.03045	136.0	4.42	43.99	38.85	1	-5.14	···	44.01	Sy1.5
NGC 5506	213.3119	-3.2075	0.00618	21.7	24.28	43.14	38.43	1	-4.71	43.20	43.19	Sy1.9
NGC 5548	214.4981	25.1368	0.01717	82.2	7.36	43.77	38.50	1	-5.27	43.46	43.63	Sy1.5
ESO 511-G030	214.8434	-26.6447	0.02239	108.9	4.41	43.80	38.39	1	-5.40	43.60	···	Sy1
Mrk 817	219.0920	58.7943	0.03145	141.5	2.74	43.82	38.57	1	-5.25	44.10	44.18	Sy1.5
NGC 5728	220.5997	-17.2532	0.0093	24.8	9.09	42.83	37.86	1	-4.97	43.45	42.64	Sy2
IC 4518A	224.4216	-43.1321	0.01626	82.0	2.79	43.35	39.20	4	-4.15	44.28	43.81	Sy2
Mrk 841	226.0050	10.4378	0.03642	162.1	3.61	44.08	···	···	···	···	44.16	Sy1
2MASX J15115979-2119015	227.9992	-21.3171	0.04461	203.2	3.24	44.20	39.51	1	-4.70	44.42	44.17	Sy1/NL
2MASX J15144217-8123377	228.6751	-81.3939	0.06837	306.9	3.09	44.54	39.09	7	-5.45	···	···	Sy1.2
MCG-01-40-001	233.3363	-8.7005	0.02271	107.5	3.27	43.65	39.61	1	-4.04	44.03	···	Sy2
NGC 5995	237.1040	-13.7578	0.02519	118.1	4.16	43.84	38.84	1	-5.00	44.41	44.26	Sy2
Mrk 1498	247.0169	51.7754	0.0547	245.8	4.24	44.49	39.60	1	-4.88	···	44.23	Sy1.9

Table 1—Continued

Name	R.A. [degree]	Dec [degree]	z	d_L [Mpc]	$F_{14-195\,\mathrm{keV}}$ [10^{-11} cgs]	$\log L_X$ [erg s^{-1}]	$\log L_R$ [erg s^{-1}]	ref.	$\log R_{rX}$	$\log L_{FIR}$ [erg s^{-1}]	$\log L_{MIR}$ [erg s^{-1}]	type
(1)	(2)	(3)	(4)	(5)	(6)	(7)	(8)	(9)	(10)	(11)	(12)	(13)
NGC 6240	253.2454	2.4009	0.02448	113.5	6.70	44.01	39.96	1	-4.05	45.08	44.25	Sy2
NGC 6300	259.2478	-62.8206	0.0037	13.1	9.70	42.30	37.31	7	-4.99	43.01	42.28	Sy2
2MASX J18074992+1120494	271.9580	11.3470	···	···	2.84	···	···	···	···	···	···	Galaxy
ESO 103-035	279.5848	-65.4276	0.01329	60.5	11.31	43.69	38.17	7	-5.52	43.25	43.64	Sy2
Fairall 51	281.2249	-62.3648	0.01417	64.1	4.26	43.32	37.88	7	-5.44	43.45	43.69	Sy1
ESO 141-G055	290.3090	-58.6703	0.036	165.4	5.34	44.24	38.44	7	-5.81	···	44.21	Sy1
NGC 6814	295.6694	-10.3235	0.00521	22.0	7.53	42.64	37.60	1	-5.03	43.13	···	Sy1.5
NGC 6860	302.1954	-61.1002	0.01488	67.5	5.28	43.46	38.00	7	-5.46	43.40	43.44	Sy1
Mrk 509	311.0406	-10.7235	0.0344	151.6	9.42	44.41	38.85	1	-5.56	···	44.36	Sy1.2
6dF J2132022-334254	323.0092	-33.7150	0.02929	131.4	4.45	43.96	37.96	1	-6.00	···	···	Sy1
1RXS J213623.1-622400	324.0963	-62.4002	0.0588	260.0	2.92	44.37	38.70	7	-5.68	···	···	Sy1
Mrk 520	330.1724	10.5524	0.02661	115.5	3.18	43.70	39.11	1	-4.60	44.43	43.90	Sy1.9
NGC 7172	330.5080	-31.8698	0.00868	31.9	17.36	43.32	37.80	1	-5.53	43.52	43.11	Sy2
NGC 7213	332.3177	-47.1667	0.00584	14.5	4.43	42.05	37.47	7	-4.58	42.39	42.48	Sy1.5
NGC 7314	338.9426	-26.0503	0.00476	15.9	5.12	42.19	37.12	1	-5.07	42.66	···	Sy1.9
NGC 7319	339.0148	33.9757	0.02251	97.3	3.93	43.65	38.92	1	-4.73	43.34	43.53	Sy2
Mrk 915	339.1938	-12.5452	0.02411	104.0	3.22	43.62	39.10	1	-4.52	···	···	Sy1
MR 2251-178	343.5242	-17.5819	0.06398	282.3	10.03	44.98	39.33	1	-5.65	···	···	Sy1
NGC 7469	345.8151	8.8740	0.01632	69.9	6.87	43.60	39.17	1	-4.44	44.73	44.18	Sy1.2
Mrk 926	346.1811	-8.6857	0.04686	203.8	11.25	44.75	39.35	1	-5.40	44.03	44.00	Sy1.5
NGC 7582	349.5979	-42.3706	0.00525	18.7	8.10	42.53	38.19	4	-4.34	43.93	43.28	Sy2
NGC 7603	349.7359	0.2440	0.02952	126.5	4.85	43.97	38.81	1	-5.16	43.93	44.28	Sy1.5

Note. — (1) source name from the *Swift*–BAT catalog; (2) J2000; (3) J2000; (4) redshift; (5) luminosity distance; (6) $14-195$ keV energy flux from the *Swift*–BAT 58-month catalog; (7) $14-195$ keV luminosity; (8) 1.4 GHz radio luminosity; (9) references to radio data; (10) hard X-ray radio loudness parameter; (11) FIR luminosity at 90 μm from the*AKARI*–FIS data; (12) MIR luminosity at 9 μm from the *AKARI*–IRC data; (13) source type as given in the 58-month *Swift*–BAT catalog (Baumgartner et al. 2010).

References. — 1. Condon et al. (1998) (NVSS); 2. Becker et al. (2003) (FIRST, Version 03Apr11); 3. Wright & Otrupcek (1990) (PKSCAT90) ; 4. Condon et al. (1996); 5. Ulvestad & Wilson (1984); 6. White & Becker (1992); 7. Mauch et al. (2008) (SUMSS V2.1: 0.843 GHz); 8. Miller et al. (1993) (4.86 GHz)

Table 2. Results of the *Fermi*–LAT data analysis for the selected sample of Seyfert galaxies

Name (1)	R.A. [degree] (2)	Dec [degree] (3)	TS (4)	UL: $\mathcal{F}(>0.1\,\mathrm{GeV})$ [10^{-9} ph cm^{-2} s^{-1}] (5)	UL2: $\mathcal{F}(>0.1\,\mathrm{GeV})$ [10^{-9} ph cm^{-2} s^{-1}] (6)	UL: $\log L_\gamma$ [erg s^{-1}] (7)	UL: L_γ/L_X (8)
Mrk 1501	2.6292	10.9749	0.0	4.3	2.6	43.6	0.065
NGC 235A	10.7200	−23.5410	9.1	7.7	5.2	42.6	0.070
Mrk 348	12.1964	31.9570	0.0	2.0	1.3	41.6	0.0055
Mrk 1148	12.9783	17.4329	0.0	3.0	1.6	43.1	0.043
Mrk 352	14.9720	31.8269	0.0	3.2	2.1	41.8	0.048
Mrk 1152	18.4587	−14.8456	1.3	3.3	1.9	43.0	0.051
Fairall 9	20.9408	−58.8057	0.0	2.3	1.5	42.7	0.020
NGC 526A	20.9766	−35.0654	0.0	1.4	0.82	41.7	0.010
ESO 297-018	24.6548	−40.0114	2.5	4.8	3.1	42.5	0.030
NGC 788	30.2769	−6.8155	2.7	4.6	2.9	41.9	0.024
Mrk 1018	31.5666	−0.2914	0.7	3.9	2.1	42.8	0.052
NGC 931	37.0603	31.3117	6.4	9.4	5.5	42.1	0.067
NGC 973	38.5838	32.5056	0.0	3.5	1.9	41.8	0.054
NGC 985	38.6574	−8.7876	0.0	2.6	1.8	42.7	0.037
ESO 416-G002	38.8061	−29.6047	8.5	4.9	3.6	43.2	0.082
ESO 198-024	39.5821	−52.1923	0.0	3.2	2.0	42.8	0.049
2MASX J02485937+2630391	42.2472	26.5109	0.0	3.5	2.1	43.1	0.043
MCG-02-08-014	43.0975	−8.5104	0.9	2.5	2.0	41.8	0.041
NGC 1142	43.8008	−0.1836	0.0	1.8	1.1	42.1	0.0082
ESO 417-G006	44.0898	−32.1856	0.0	1.8	1.2	41.6	0.027
NGC 1194	45.9546	−1.1037	6.2	3.9	3.1	41.8	0.045
RX J0311.3-2046	47.8284	−20.7717	0.0	3.3	2.0	43.2	0.052
NGC 1365	53.4016	−36.1404	1.1	4.6	2.6	40.9	0.031
ESO 548-G081	55.5155	−21.2444	0.0	5.2	2.6	42.0	0.054
ESO 549-G049	60.6070	−18.0480	1.1	4.7	2.5	42.5	0.079
UGC 03142	70.9450	28.9718	1.6	9.0	6.3	42.6	0.079
2MASX J04440903+2813003	71.0376	28.2168	7.4	11.9	8.0	42.1	0.085
MCG-01-13-025	72.9229	−3.8094	3.2	3.1	2.3	41.9	0.043
CGCG 420-015	73.3573	4.0616	0.0	3.6	2.1	42.5	0.059
2MASX J05054575-2351139	76.4405	−23.8539	4.2	7.8	4.2	43.0	0.055
CGCG 468-002NED01	77.0820	17.3630	0.0	6.1	3.0	42.2	0.10
IRAS 05078+1626	77.6896	16.4989	0.0	3.1	1.7	42.0	0.015
2MASX J05151978+1854515	78.8324	18.9143	0.0	5.4	3.1	···	0.071
Ark 120	79.0476	−0.1498	0.0	2.4	1.6	42.4	0.016
ESO 362-18	79.8993	−32.6578	7.1	8.0	4.6	42.1	0.068
2MASX J05442257+5907361	86.0941	59.1267	0.0	2.9	1.9	43.1	0.048
NGC 2110	88.0474	−7.4562	0.1	5.2	2.2	41.4	0.0076
MCG+08-11-011	88.7234	46.4393	0.0	3.3	1.9	42.1	0.011
2MASX J05580206-3820043	89.5083	−38.3346	0.0	7.1	3.5	42.9	0.11
ESO 005-G004	91.4235	−86.6319	0.0	2.8	1.6	40.8	0.033
ESO 121-IG028	95.9400	−60.9790	0.0	2.2	1.2	42.6	0.036
ESO 426-G002	95.9434	−32.2166	0.7	5.9	3.4	42.5	0.095
ESO 490-IG026	100.0487	−25.8954	0.1	3.4	2.6	42.3	0.039
2MASX J06411806+3249313	100.3252	32.8254	0.5	4.7	3.3	43.0	0.055
Mrk 6	103.0511	74.4271	0.0	3.7	2.3	42.1	0.026
Mrk 79	115.6367	49.8097	2.5	6.1	3.2	42.5	0.057
2MASX J07595347+2323241	119.9728	23.3901	0.3	3.9	2.2	42.5	0.052
IC 0486	120.0874	26.6135	10.6	9.3	6.3	42.8	0.11
Mrk 1210	121.0244	5.1138	4.4	7.8	4.5	42.2	0.063

Table 2—Continued

Name	R.A. [degree]	Dec [degree]	TS	UL: $\mathcal{F}(>0.1\,\mathrm{GeV})$ [10^{-9} ph cm^{-2} s^{-1}]	UL2: $\mathcal{F}(>0.1\,\mathrm{GeV})$ [10^{-9} ph cm^{-2} s^{-1}]	UL: $\log L_\gamma$ [erg s^{-1}]	UL: L_γ/L_X
(1)	(2)	(3)	(4)	(5)	(6)	(7)	(8)
Fairall 272	125.7546	−4.9349	0.1	3.3	2.1	42.2	0.030
Mrk 704	139.6084	16.3053	0.0	3.5	2.0	42.5	0.046
MCG-01-24-012	140.1927	−8.0561	0.0	2.3	1.5	42.0	0.024
MCG+04-22-042	140.9292	22.9090	0.0	2.4	1.6	42.4	0.025
Mrk 110	141.3036	52.2863	0.0	3.0	1.9	42.6	0.023
MCG-05-23-016	146.9173	−30.9489	0.0	2.4	1.5	41.2	0.0053
NGC 3081	149.8731	−22.8263	0.0	4.2	2.5	41.2	0.021
ESO 263-G013	152.4509	−42.8112	0.0	5.6	3.6	42.8	0.073
NGC 3227	155.8774	19.8651	3.1	5.2	2.6	41.3	0.020
NGC 3281	157.9670	−34.8537	3.3	8.0	5.1	41.9	0.040
2MASS J10315431-1416514	157.9763	−14.2809	8.9	7.5	5.2	43.8	0.094
NGC 3393	162.0977	−25.1621	8.2	5.8	4.3	42.0	0.098
Mrk 417	162.3789	22.9644	1.2	6.5	3.7	42.9	0.084
NGC 3516	166.6979	72.5686	4.3	6.8	3.4	41.7	0.024
NGC 3783	174.7572	−37.7386	3.3	7.5	4.7	41.4	0.017
UGC 06728	176.3168	79.6815	0.0	2.3	1.4	41.1	0.037
2MASX J11454045-1827149	176.4186	−18.4543	0.6	5.1	2.8	42.8	0.045
NGC 4051	180.7901	44.5313	0.0	2.7	1.7	40.6	0.031
Ark 347	181.1237	20.3162	5.0	6.7	3.1	42.6	0.10
NGC 4138	182.3741	43.6853	1.5	4.3	2.7	40.6	0.061
NGC 4151	182.6357	39.4057	0.0	3.1	2.1	40.3	0.0025
NGC 4235	184.2912	7.1916	0.7	5.3	3.2	41.4	0.073
NGC 4388	186.4448	12.6621	0.0	3.5	2.1	40.7	0.0055
NGC 4395	186.4538	33.5468	0.0	3.3	2.1	39.6	0.055
NGC 4507	188.9026	−39.9093	1.1	6.8	4.1	42.1	0.016
ESO 506-G027	189.7275	−27.3078	0.0	3.0	1.8	42.3	0.014
LEDA 170194	189.7762	−16.1797	0.3	5.3	3.1	42.9	0.052
NGC 4593	189.9143	−5.3443	5.1	7.6	3.6	41.7	0.037
NGC 4686	191.6661	54.5342	0.0	2.0	1.3	41.8	0.032
SBS 1301+540	195.9978	53.7917	0.3	3.9	2.5	42.6	0.049
NGC 4939	196.0600	−10.3396	0.1	4.0	1.9	41.4	0.067
ESO 323-G077	196.6089	−40.4146	0.0[a]	6.5	5.3	42.1	0.066
			26.7	[Flux] 8.2 ± 2.7[b] ,	[Index] $\Gamma = 2.21\pm0.14$[b]	42.3	0.11
NGC 4992	197.2733	11.6341	0.0	3.9	2.7	42.4	0.030
MCG-06-30-015	203.9741	−34.2956	0.0	4.2	2.4	41.2	0.029
NGC 5252	204.5665	4.5426	0.0	2.7	1.4	42.2	0.010
IC 4329A	207.3303	−30.3094	2.5	7.6	4.6	42.4	0.011
Mrk 279	208.2644	69.3082	3.6	5.1	3.0	42.7	0.050
NGC 5506	213.3119	−3.2075	0.0	4.0	2.4	41.0	0.0071
NGC 5548	214.4981	25.1368	0.0	3.7	2.4	42.1	0.022
ESO 511-G030	214.8434	−26.6447	0.0	2.6	1.6	42.2	0.025
Mrk 817	219.0920	58.7943	0.0	2.4	1.6	42.4	0.038
NGC 5728	220.5997	−17.2532	2.2	7.5	3.9	41.4	0.035
IC 4518A	224.4216	−43.1321	0.6	7.3	3.5	42.4	0.11
Mrk 841	226.0050	10.4378	0.0	31.2	14.9	43.7	0.37
2MASX J15115979-2119015	227.9992	−21.3171	7.3	11.7	7.5	43.4	0.16
2MASX J15144217-8123377	228.6751	−81.3939	5.3	12.2	7.4	43.8	0.17
MCG-01-40-001	233.3363	−8.7005	0.4	6.5	3.4	42.6	0.086
NGC 5995	237.1040	−13.7578	0.0	2.9	2.0	42.3	0.030

Table 2—Continued

Name	R.A. [degree]	Dec [degree]	TS	UL: $\mathcal{F}(>0.1\,\mathrm{GeV})$ $[10^{-9}$ ph cm^{-2} s$^{-1}]$	UL2: $\mathcal{F}(>0.1\,\mathrm{GeV})$ $[10^{-9}$ ph cm^{-2} s$^{-1}]$	UL: $\log L_\gamma$ [erg s^{-1}]	UL: L_γ/L_X
(1)	(2)	(3)	(4)	(5)	(6)	(7)	(8)
Mrk 1498	247.0169	51.7754	1.1	6.0	3.3	43.3	0.061
NGC 6240	253.2454	2.4009	0.0	4.2	2.4	42.4	0.027
NGC 6300	259.2478	−62.8206	5.8	12.2	6.5	41.0	0.054
2MASX J18074992+1120494	271.9580	11.3470	4.7	11.6	6.0	···	0.18
ESO 103-035	279.5848	−65.4276	0.3	2.9	2.3	41.7	0.011
Fairall 51	281.2249	−62.3648	0.5	5.9	3.7	42.1	0.060
ESO 141-G055	290.3090	−58.6703	0.0	2.5	1.8	42.6	0.020
NGC 6814	295.6694	−10.3235	0.0[c]	6.6	3.8	41.2	0.038
			25.6	[Flux] 16 ± 5[d] ,	[Index] $\Gamma=2.50\pm0.15$[d]	41.6	0.093
NGC 6860	302.1954	−61.1002	0.0	2.6	1.7	41.8	0.022
Mrk 509	311.0406	−10.7235	0.9	3.5	2.7	42.6	0.016
6dFJ2132022-334254	323.0092	−33.7150	0.0	2.1	1.3	42.3	0.020
1RXS J213623.1-622400	324.0963	−62.4002	4.3	4.8	3.6	43.2	0.071
Mrk 520	330.1724	10.5524	0.0	3.1	2.2	42.3	0.042
NGC 7172	330.5080	−31.8698	2.8	4.5	3.4	41.4	0.011
NGC 7213	332.3177	−47.1667	4.5	6.7	3.5	40.9	0.065
NGC 7314	338.9426	−26.0503	2.5	6.0	3.3	40.9	0.051
NGC 7319	339.0148	33.9757	0.0	2.3	1.5	42.1	0.025
Mrk 915	339.1938	−12.5452	0.0	4.1	2.4	42.4	0.055
MR 2251-178	343.5242	−17.5819	0.0	2.0	1.4	42.9	0.0085
NGC 7469	345.8151	8.8740	0.0	2.4	1.6	41.8	0.015
Mrk 926	346.1811	−8.6857	0.0	2.5	1.5	42.7	0.0094
NGC 7582	349.5979	−42.3706	0.3	5.8	3.5	41.0	0.031
NGC 7603	349.7359	0.2440	0.0	3.3	2.0	42.4	0.029

[a]The case in which the association of ESO 323-G077 with 2FGL J1306.9–4028 is actually the result of a chance spatial coincidence. 2FGL J1306.9–4028 is included as a background source in the model.

[b]Assuming that ESO 323-G077 is detected by the LAT as 2FGL J1306.9–4028.

[c]The case in which the association of NGC 6814 with 2FGL J1942.5–1024 is actually the result of a chance spatial coincidence. 2FGL J1942.5–1024 is included as a background source in the model.

[d]Assuming that NGC 6814 is detected by the LAT as 2FGL J1942.5–1024.

Note. — (1) Source name from the *Swift*–BAT catalog; (2) Right ascension J2000; (3) Declination J2000; (4) TS of the γ-ray event excess using *Fermi*–LAT data above 0.2 GeV at the source position; (5) 95% C.L. upper limits for the photon flux above 0.1 GeV assuming photon index $\Gamma = 2.5$; (6) 95% C.L. upper limits for the photon flux above 0.1 GeV assuming photon index $\Gamma = 2.2$; (7) 95% C.L. upper limits for γ-ray luminosity in a range between 0.1 and 10 GeV based on the results of (5), assuming photon index $\Gamma = 2.5$; (8) upper limits for γ-ray–to–hard X-ray luminosity based on the results of (5), assuming photon index $\Gamma = 2.5$;

Table 3. Starburst galaxies discussed in the paper

Name	d_L [Mpc]	$\mathcal{F}(> 0.1\,\mathrm{GeV})$ [10^{-9} ph cm^{-2} s^{-1}]	$\log L_\gamma$ [erg s^{-1}]	$F_{14-195\,\mathrm{keV}}$ [10^{-11} cgs]	$\log L_\mathrm{X}$ [erg s^{-1}]	$\log L_\mathrm{R}$ [erg s^{-1}]	$\log R_\mathrm{rX}$	$\log L_\mathrm{FIR}$ [erg s^{-1}]	$\log L_\mathrm{MIR}$ [erg s^{-1}]
(1)	(2)	(3)	(4)	(5)	(6)	(7)	(8)	(9)	(10)
NGC 253	2.5	12.6 ± 2.0	39.8	···	···	37.77	···	43.38	42.75
M82	3.4	15.4 ± 1.9	40.2	···	···	38.17	···	43.83	···
NGC 4945	3.7	8.5 ± 2.8	40.1	30.10	41.69	38.18	-3.51	43.53	42.68
NGC 1068	16.7	6.4 ± 2.0	41.2	3.38	42.05	39.37	-2.68	44.35	44.44

Note. — (1) source name; (2) luminosity distance; (3) γ-ray photon flux above 0.1 GeV taken from Ackermann et al. (2011b); (4) γ-ray luminosity above 0.1 GeV taken from Ackermann et al. (2011b); (5) $14-195$ keV energy flux from the *Swift*–BAT 58-month catalog; (6) $14-195$ keV luminosity; (7) 1.4 GHz radio luminosity; (8) hard X-ray radio loudness parameter; (9) FIR luminosity at 90 μm from the *AKARI*–FIS data for NGC 1068, and at 60 μm from the IRAS data for others; (10) MIR luminosity at 9 μm from the *AKARI*–IRC data.